Eddy stirring in the Southern Ocean

A. C. Naveira Garabato,[1] R. Ferrari,[2] and K. L. Polzin[3]

Received 21 November 2010; revised 8 June 2011; accepted 6 July 2011; published 17 September 2011.

[1] There is an ongoing debate concerning the distribution of eddy stirring across the Antarctic Circumpolar Current (ACC) and the nature of its controlling processes. The problem is addressed here by estimating the isentropic eddy diffusivity κ from a collection of hydrographic and altimetric observations, analyzed in a mixing length theoretical framework. It is shown that, typically, κ is suppressed by an order of magnitude in the upper kilometer of the ACC frontal jets relative to their surroundings, primarily as a result of a local reduction of the mixing length. This observation is reproduced by a quasi-geostrophic theory of eddy stirring across a broad barotropic jet based on the scaling law derived by Ferrari and Nikurashin (2010). The theory interprets the observed widespread suppression of the mixing length and κ in the upper layers of frontal jets as the kinematic consequence of eddy propagation relative to the mean flow within jet cores. Deviations from the prevalent regime of mixing suppression in the core of upper-ocean jets are encountered in a few special sites. Such 'leaky jet' segments appear to be associated with sharp stationary meanders of the mean flow that are generated by the interaction of the ACC with major topographic features. It is contended that the characteristic thermohaline structure of the Southern Ocean, consisting of multiple upper-ocean thermohaline fronts separated and underlaid by regions of homogenized properties, is largely a result of the widespread suppression of eddy stirring by parallel jets.

Citation: Naveira Garabato, A. C., R. Ferrari, and K. L. Polzin (2011), Eddy stirring in the Southern Ocean, *J. Geophys. Res.*, *116*, C09019, doi:10.1029/2010JC006818.

1. Introduction

[2] The Southern Ocean plays a pivotal role in the global overturning circulation. The absence of continental barriers in the latitude band of Drake Passage permits the existence of the Antarctic Circumpolar Current (ACC), which is supported geostrophically by sloping isopycnals and serves as the main conduit for oceanic exchanges between the three major ocean basins. Coupled to this eastward, multi-jet flow, a meridional circulation exists in which Circumpolar Deep Water (CDW) with primordial sources in the North Atlantic, upwells along the poleward-shoaling isopycnals of the ACC and is returned equatorward in a double overturning cell. This pattern of overturning can be surmised from a meridional section of almost any hydrographic or biogeochemical property across the Southern Ocean, such as the section of salinity shown in Figure 1a. The Upper classes of CDW are entrained into the upper-ocean mixed layer within the ACC itself and subsequently flow northward as Antarctic Surface Water, which subducts into Antarctic Intermediate Water and Subantarctic Mode Water near the current's northern rim (the upper cell). The Lower classes of CDW are transported southward beyond the ACC and enter the system of subpolar cyclonic gyres and westward-flowing slope jets encircling the Antarctic continent. There, CDW replenishes and mixes with Antarctic surface and shelf waters, ultimately resulting in the formation and northward export of Antarctic Bottom Water (the lower cell). This meridional circulation is a key step in the vertical transfer of water masses and physical tracers required to close global overturning, and underlies the Southern Ocean's disproportionate importance in the ventilation of the deep ocean. *Rintoul et al.* [2001] and *Olbers et al.* [2004] provide reviews of the contemporary state of knowledge on the Southern Ocean circulation, its function in the global ocean, and its essential dynamics.

[3] Beyond the above qualitative description, significant uncertainties remain on the rate, structure and driving mechanisms of the Southern Ocean overturning. The main thrust of progress has been provided by a large body of work articulated around residual mean theory [e.g., *Marshall*, 1997; *Speer et al.*, 2000; *Karsten and Marshall*, 2002; *Bryden and Cunningham*, 2003; *Marshall and Radko*, 2003, 2006; *Olbers and Visbeck*, 2005]. A fundamental result is the description of the Southern Ocean overturning as the residual arising from the partial cancelation between two distinct circulations: a wind-forced Ekman overturning acting to tilt ACC isopycnals upward, and an overturning in the opposite sense induced by geostrophic eddies arising from baroclinic

[1]University of Southampton, National Oceanography Centre, Southampton, UK.
[2]Department of Earth, Atmospheric and Planetary Sciences, Massachusetts Institute of Technology, Cambridge, Massachusetts, USA.
[3]Physical Oceanography Department, Woods Hole Oceanographic Institution, Woods Hole, Massachusetts, USA.

0148-0227/11/2010JC006818

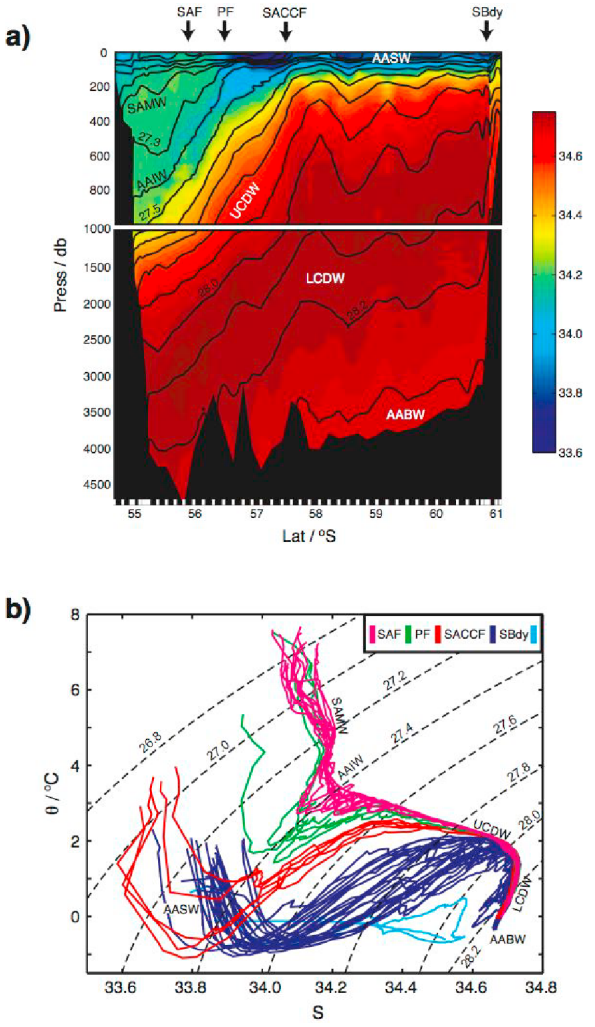

Figure 1. (a) Meridional section of salinity (in color) across eastern Drake Passage (section location indicated as WOCE SR1b in Figure 2a). Neutral density contours (contour interval = 0.1 kg m^{-3}) are shown in black, and the major water masses labeled (AABW = Antarctic Bottom Water; AAIW = Antarctic Intermediate Water; AASW = Antarctic Surface Water; LCDW = Lower Circumpolar Deep Water; SAMW = Subantarctic Mode Water; UCDW = Upper Circumpolar Deep Water). Station positions are indicated by the white tick marks at the base of the figure. The locations of the ACC fronts (PF = Polar Front; SACCF = Southern ACC Front; SAF = Subantarctic Front) and its Southern Boundary (SBdy) are shown by the arrows at the top of the figure. (b) θ-S diagram corresponding to Figure 1a. θ-S curves are colored according to the interfrontal zone in which they lie. Selected isoneutral contours are displayed in black. Water masses and fronts are labeled as in Figure 1a.

instability and acting to slump isopycnals. The wind-driven Ekman overturning consists of upwelling (downwelling) to the south (north) of the ACC's axis, northward flow in a surface Ekman layer, and a return southward geostrophic flow below the crests of the topographic barriers in the ACC's path. In this way, it contributes importantly to the lower cell of the Southern Ocean overturning, as well as to the northward limb of the overturning's upper cell. The influence of the eddy-induced circulation is thought to be particularly significant above the level of the topography (roughly in the top ~2500 m), where it sustains the upwelling of Upper CDW and promotes intermediate water subduction. Water mass conversion through diapycnal flow is often assumed to be largely confined to the upper ocean, where it is supported by air-sea buoyancy exchanges and eddy-induced diapycnal fluxes, although the extent to which this assumption holds has been questioned [e.g., *Garabato et al.*, 2004].

[4] The central difficulty in translating this theoretical picture of the Southern Ocean overturning's dynamics into an accurate diagnostic of the circulation's rate and structure pertains to the eddy-induced contribution to the overturning. In contrast to the wind-driven Ekman circulation, which can be estimated from gross knowledge of the wind stress and the topography, the eddy-induced overturning arises from transient eddy fluctuations on scales of O(100 km) that are difficult to quantify in observations. A common approach is to relate the eddy-induced circulation to a downgradient flux of potential vorticity (PV) resulting from eddy stirring, and to parameterize this flux with a flux-gradient relation [e.g., *Rhines and Young*, 1982]. In terms of a generalized tracer ϕ,

$$\overline{v'\phi'} = -\kappa \frac{\partial \overline{\phi}}{\partial y}, \tag{1}$$

where the overbars indicate zonal (along-stream) and temporal averages on an isopycnal layer, the primes indicate deviations from those averages, the tracer gradient is assumed to be meridional (cross-stream), and κ is an isopycnal (strictly, isentropic, but taken here to be equivalent) eddy diffusivity characterizing the rate of eddy stirring. We note that the feedback of the tracer flux onto the mean circulation is through its divergence, ∂_y ($\overline{v'\phi'}$), such that the spatial distribution of κ relative to the background tracer gradient assumes a key role. In the context of the Southern Ocean circulation, it is the relative spatial variability of κ and the large-scale isopycnal PV gradient that sets the rate and structure of the eddy-induced contribution to the overturning.

[5] In the virtual absence of direct observations of eddy stirring in the Southern Ocean, attempts at determining κ have resorted to a wide range of approaches and yielded diverse results. The methods, assumptions and outcomes of these past studies are discussed in detail in section 4, against the backdrop of our own results. We caution, though, that the focus of the present study is on isopycnal diffusivities for passive and active tracers. As flows in the ocean interior are aligned with isopycnal surfaces, one may safely assume that tracer fluctuations are primarily generated by along-isopycnal stirring of large-scale tracer gradients. The same presumption cannot be made for buoyancy fluctuations, and hence the diffusivity for buoyancy can be quite different, in particular in its vertical structure (for a more in-depth discussion, see *Smith and Marshall* [2009]). This distinction should be kept in mind when comparing our results to previous literature.

[6] With this caveat noted, it suffices to say for now that previous studies of eddy stirring in the Southern Ocean and beyond may be loosely grouped into two categories: those that point to an enhancement of κ where eddy kinetic energy

(EKE) is highest, i.e., at the surface and at the core of jets [e.g., *Holloway*, 1986; *Keffer and Holloway*, 1988; *Stammer*, 1998]; and others that contend that κ is instead enhanced along a Rossby wave critical layer (at which the phase speed of the waves approximately matches the mean zonal flow speed) lying at mid depth in the ACC core and surfacing on the current's equatorward flank [e.g., *Killworth*, 1997; *Treguier*, 1999; *Cerovečki et al.*, 2009; *Smith and Marshall*, 2009; *Abernathy et al.*, 2009]. Both of these contrasting views can draw some support from observational analyses. *Ferrari and Nikurashin* [2010] address the controversy from a theoretical standpoint by arguing that the spatial variability of κ is shaped both by the magnitude of the EKE and the speed of the waves relative to the mean flow. In so doing, they derive a scaling law that quantifies whether specific jets are regions of vigorous or reduced mixing depending on the relative importance of the two effects.

[7] Here we contend that meridional transects of hydrographic properties (e.g., Figure 1a) provide significant insight into the spatial structure of κ across the Southern Ocean. To illustrate this point, consider the potential temperature-salinity (θ-S) diagram corresponding to the section in Figure 1a. This θ-S diagram (Figure 1b) displays many features that will be familiar to anyone who has examined hydrographic measurements from the Southern Ocean, e.g., well-defined clusters of θ-S curves that characterize the ACC's interfrontal zones above the core of CDW, gaps in thermohaline space that occur at the fronts within the same range of densities, and comparative homogeneity in the properties of the bulk of CDW. This θ-S distribution hints at a marked *suppression* of eddy stirring in the upper and intermediate layers of the ACC fronts relative to deeper levels and surrounding regions, and appears to conflict with the aforementioned view that κ may be enhanced near the surface and at the core of jets.

[8] In this article, we estimate the structure of κ in the Southern Ocean by combining a set of hydrographic sections across the ACC and spatially coincident altimetric measurements within a mixing length theoretical framework. We focus exclusively on the diffusivity characterizing cross-stream eddy stirring, for the generally much larger along-stream diffusivities [*Smith*, 2005] are irrelevant to meridional transport across the Southern Ocean. Mixing length theory [e.g., *Prandtl*, 1925] asserts that κ may be represented as the product of an eddy velocity scale U_e and an eddy mixing length scale L_{mix}, such as

$$\kappa = c_e U_e L_{mix}, \tag{2}$$

where c_e is a constant metric of the efficiency of the stirring process. We show that, typically, κ is strongly suppressed in the upper O(1 km) of the ACC frontal jets relative to their surroundings and, like *Ferrari and Nikurashin* [2010], we interpret the spatial distribution of κ as resulting from modulation of L_{mix} by eddy-mean flow interactions. We show, further, that the characteristic barrier behavior of upper-ocean jets breaks down at a few special sites. There, significant departures from parallel flow conditions and the absence of a clear separation between mean and eddy length scales appear to mark the onset of a distinct mixing regime, in which jets become leaky and mixing is no longer suppressed. It is in such leaky jet segments that high values of κ are seen to occur in conjunction with large isopycnal PV gradients, suggesting that those sites contribute disproportionally to the eddy-induced component of the Southern Ocean overturning.

[9] The paper is organized as follows. Section 2 introduces the collection of data sets used in this study. In section 3, we discuss the application of our methodology to the data, and the resulting distributions of L_{mix}, U_e and κ. Theoretical interpretations of these distributions are presented and assessed in section 4. Lastly, section 5 presents the conclusions of our work and considers its implications for the thermohaline structure and overturning circulation of the Southern Ocean.

2. Data

[10] The work presented here makes use of several observational data sets. A collection of meridional high-quality ("high-quality" in this context refers to temperature and salinity accuracies of at least WOCE standard, i.e., 0.001 and 0.003, respectively) hydrographic sections across the Southern Ocean is at the heart of our calculation of L_{mix}. This includes only repeat transects or sections with particularly small (<30 km) station spacing. Experience gained by subsampling finely resolved transects suggests that, in the absence of repeats, a considerably coarser station spacing compromises the resolution of lateral structures in L_{mix} (see Appendix A). We analyze sections conducted at five different World Ocean Circulation Experiment (WOCE) transect locations spanning a wide range of mean flow (Figure 2a) and EKE (Figure 2b) regimes: western (WOCE S1) and eastern (WOCE SR1b) Drake Passage, the western Indian Ocean south of Africa (WOCE I6S), the eastern Indian Ocean (WOCE I8S), and the western Pacific Ocean south of Tasmania (WOCE SR3). Some details of the section occupations examined here are listed in Table 1. Our analysis of the latter three transects is restricted to the region of monotonically increasing geopotential height toward the north, for reasons that will become apparent in section 3.

[11] Our estimation of U_e relies primarily on the analysis of a 15-year (1992–2007) time series of weekly sea surface height anomaly fields optimally interpolated to a $\frac{1}{3}^\circ$ Mercator grid by Aviso from TOPEX/POSEIDON, Jason-1, ERS-1, ERS-2 and Envisat altimetric observations [*Traon et al.*, 2003]. This data set is used in conjunction with an estimate of the absolute sea surface dynamic topography with fine mesoscale resolution obtained by *Maximenko and Niiler* [2005] from drifter, satellite altimetric, NCEP/NCAR reanalysis wind and GRACE gravity data. We estimate the subsurface flow by combining these sea surface topographic data sets with the hydrographic sections introduced above, in the manner described in section 3.2.

3. Structure of the Isentropic Eddy Diffusivity in the Southern Ocean Diagnosed From Observations

3.1. Estimates of the Eddy Mixing Length Scale L_{mix} From Hydrographic Sections

[12] Our method for estimating L_{mix} rests on the mixing length arguments of *Armi and Stommel* [1983] [see also

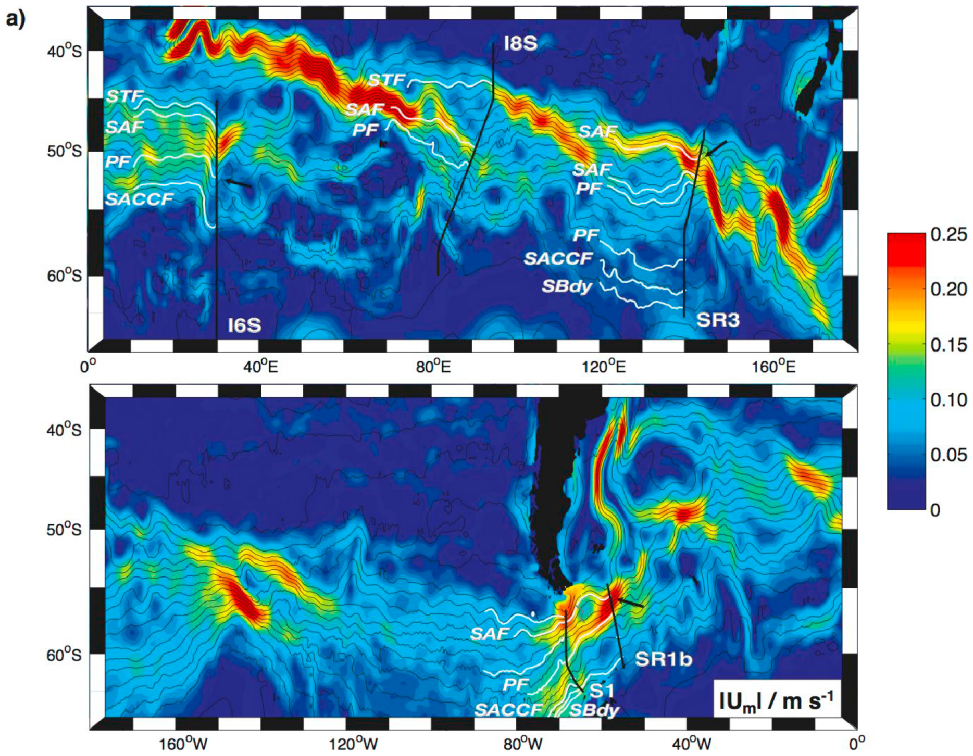

Figure 2. (a) Surface flow speed (in color) estimated from the mean dynamic topography of *Maximenko and Niiler* [2005]. Mean dynamic topography contours at intervals of 0.1 m are shown by the thin black lines in all panels. The locations of the hydrographic sections analyzed in this study are indicated by the thick black lines in all panels and labeled in Figure 2a. The thick grey line in Drake Passage marks the position of the ISOS section discussed in section 4.1. The white lines in Figures 2a–2d show segments (extending over 20° of longitude upstream of each section) of the mean dynamic topography contours associated with the cores of frontal jets at each of the hydrographic transects, and are labeled in Figure 2a with the standard frontal terminology (STF = Subtropical Front; see caption of Figure 1 for other definitions). These lines are displayed in black in Figure 2e for clarity. The black arrows in all panels indicate the positions of the leaky jets sampled by the hydrographic sections. (b) Eddy kinetic energy (in color) calculated from the Aviso gridded altimetry product. (c) Inverse suppression factor $[1 + 4U_0^2\, EKE^{-1}]^{-1}$ (in color), calculated as described in section 5. The jets in the hydrographic sections that exhibit mixing suppression are indicated by open squares, and leaky jets are marked by open circles. (d) Zonal speed of propagating eddies (in color) estimated from the Aviso gridded altimetry product by Chris Hughes. (e) Okubo-Weiss parameter D (in color) calculated from Maximenko and Niiler's mean dynamic topography.

Ferrari and Polzin, 2005], according to which L_{mix} may be defined as

$$L_{mix} = \frac{\theta_{rms}}{|\nabla_n \theta_m|}, \tag{3}$$

where θ_{rms} is the rms potential temperature fluctuation along a neutral surface arising from eddy stirring of the large-scale potential temperature θ_m, and ∇_n is the gradient operator on the same neutral surface. This definition is formally valid to the extent that tracer fluctuations are generated by local stirring of the large-scale tracer gradient (i.e., advection of tracer variance from regions upstream is assumed to be weak), and insofar as $|\nabla_n \theta_m|$ varies slowly over the eddy mixing length L_{mix} (i.e., a scale separation between eddy and mean flow scales is assumed). While the first assumption appears to hold in numerical models [*Abernathy et al.*, 2009], it is difficult to extrapolate to the real ocean because models and observations are too coarse to quantify tracer variance budgets over large regions. The second assumption might be violated where jets are particularly narrow and there is no distinction between mean and eddy length scales. We chose to proceed and presume that both assumptions hold. Verification of the assumptions will be done *a posteriori*, to the extent that spatial variations in our estimates of L_{mix} can be related to local flow and tracer statistics.

[13] We note that this description of lateral mixing is, by assumption, distinct from that put forward by *Joyce et al.* [1978] in the context of a high-spatial-resolution survey of the PF that was part of the International Southern Ocean Studies (ISOS). Whereas our framework assumes that thermohaline variability on isoneutrals arises passively from the mesoscale eddy-induced filamentation of background

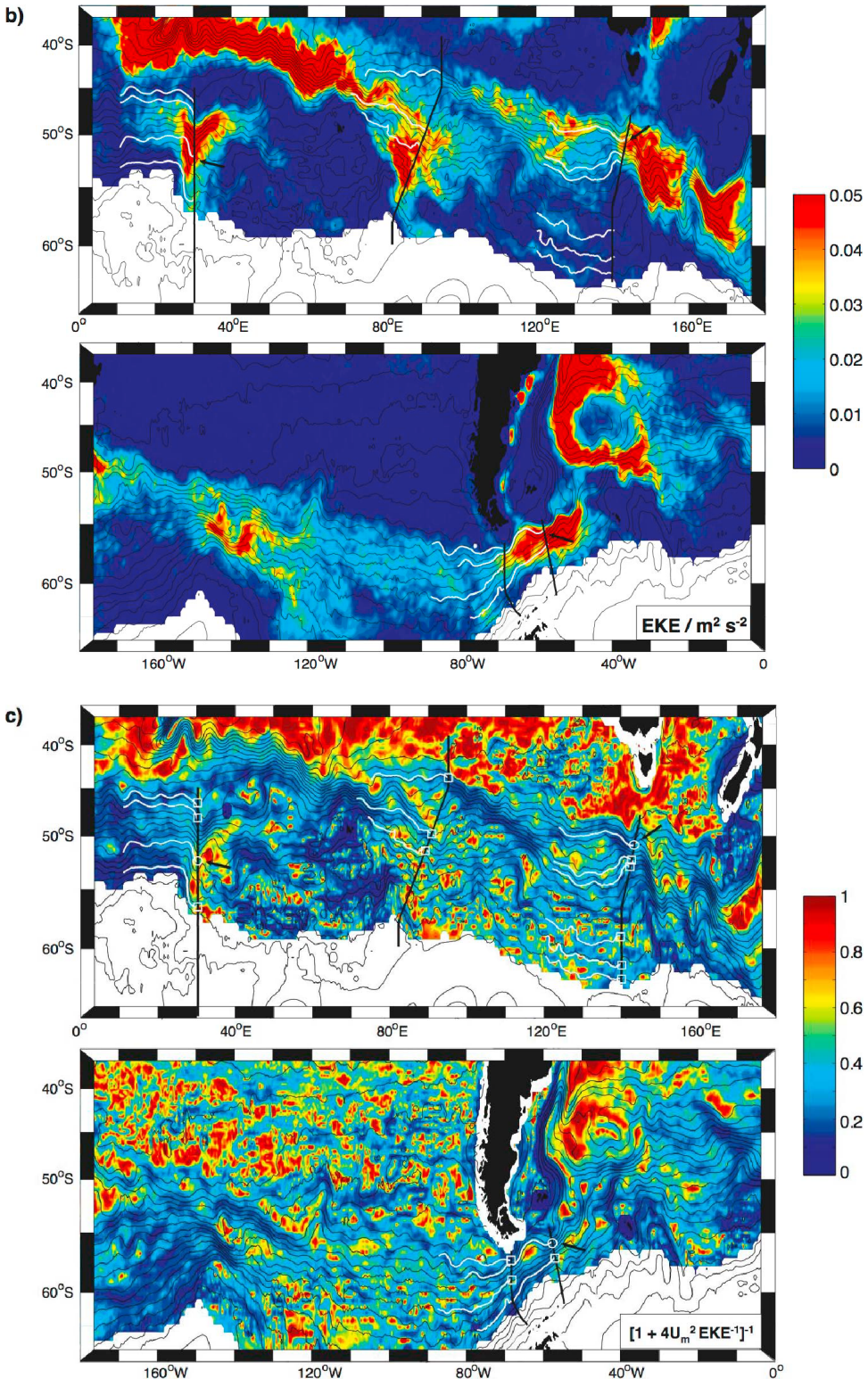

Figure 2. (continued)

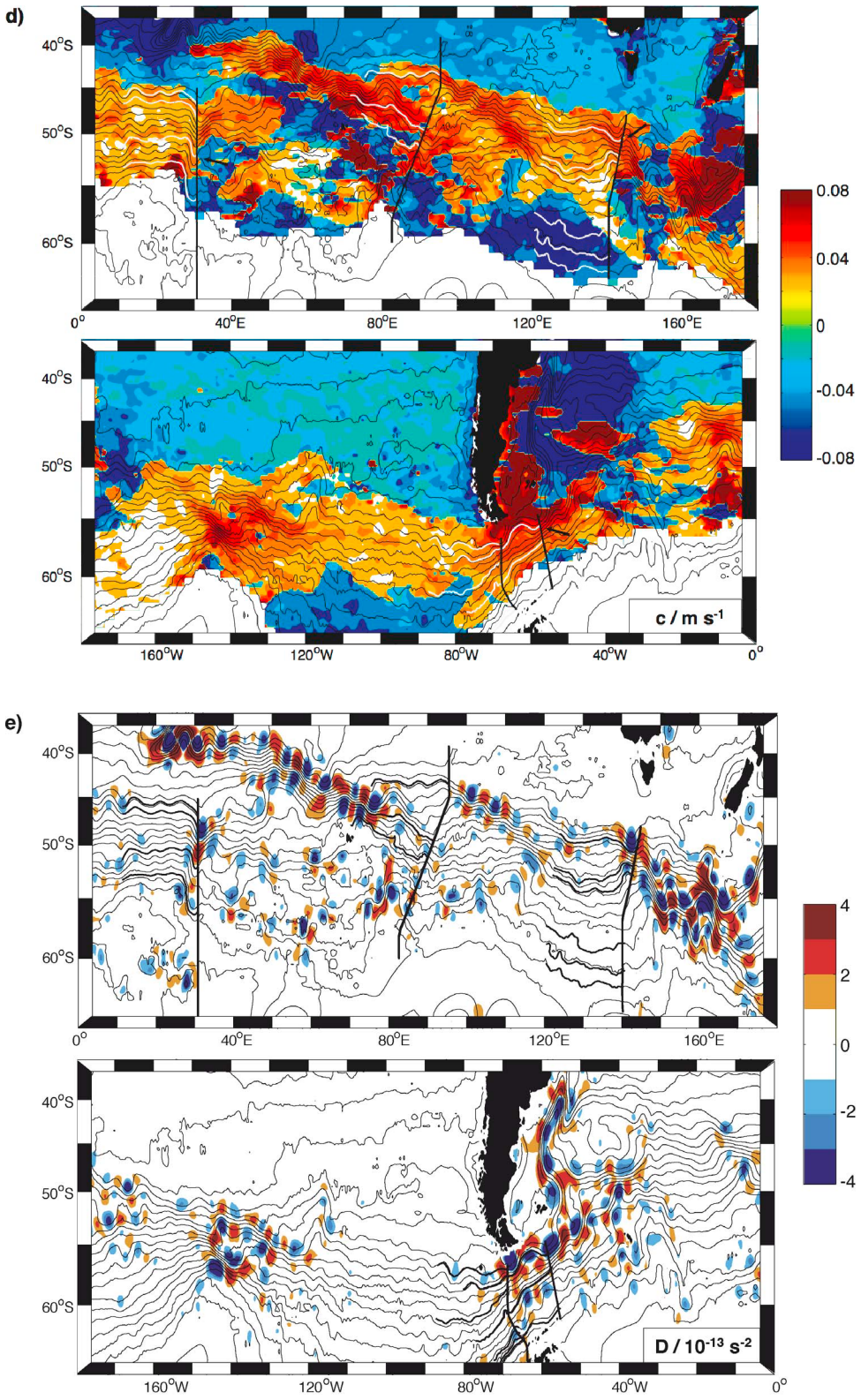

Figure 2. (continued)

Table 1. Meridional High-Quality CTD Sections Analyzed in This Study[a]

WOCE Section Code	Nominal Location	Vessel	Dates of Occupation
S1	Western Drake Passage	RRS *James Clark Ross*	18–26 Mar 1999
SR1b	Eastern Drake Passage	RRS *James Clark Ross*	21–26 Nov 1993
		RRS *James Clark Ross*	15–21 Nov 1994
		RRS *James Clark Ross*	15–20 Nov 1996
		RRS *James Clark Ross*	29 Dec 1997 to 7 Jan 1998
		RRS *James Clark Ross*	22–28 Nov 2000
		RRS *James Clark Ross*	20–26 Nov 2001
		RRS *James Clark Ross*	27 Dec 2002 to 1 Jan 2003
		RRS *James Clark Ross*	11–15 Dec 2003
		RRS *James Clark Ross*	2–8 Dec 2004
		RRS *James Clark Ross*	7–12 Dec 2005
I6S	Western Indian Ocean	NO *Marion Dufresne*	5 Feb to 10 Mar 1993
		NO *Marion Dufresne*	21 Feb to 21 Mar 1996
I8S	Eastern Indian Ocean	R/V *Knorr*	5–28 Dec 1994
		R/V *Roger Revelle*	15 Feb to 13 Mar 2007
SR3	Western Pacific Ocean	RSV *Aurora Australis*	8–26 Oct 1991
		RSV *Aurora Australis*	12–28 Mar 1993
		RSV *Aurora Australis*	1–16 Jan 1994
		RSV *Aurora Australis*	19 Jan to 2 Feb 1995
		RSV *Aurora Australis*	17 Jul to 27 Aug 1995
		RSV *Aurora Australis*	1 Sep to 21 Sep 1996
		RSV *Aurora Australis*	29 Oct to 28 Nov 2001

[a]The nominal location, vessel and dates of each occupation are listed.

$\theta - S$ gradients (e.g., as found by *Smith and Ferrari* [2009] in the eastern subtropical North Atlantic), *Joyce et al.* [1978] contend that interleaving features actively enhance thermohaline variability through double diffusive processes that cause the features to slope across neutral surfaces. The rationale and justification of our framework and the extent to which it affects our results are discussed in Appendix B.

[14] Along each hydrographic section, we calculate θ_m and θ_{rms} on discrete neutral surfaces separated by an interval of 0.02 kg m^{-3} in the neutral density variable $\gamma^n$of [*Jackett and McDougall*, 1997]. This involves mapping the measured θ profiles, which are provided in a 2 dbar pressure grid, to the selected γ^n surfaces using linear interpolation. We wish to distinguish between spatial θ anomalies caused by the meandering of streamlines, which in the ACC are aligned with horizontal contours of hydrographic properties to a very good approximation [*Sun and Watts*, 2001], and anomalies associated with the genuine eddy-induced translation of water parcels across streamlines, which ultimately leads to cross-stream mixing when those anomalies are eroded by small-scale mixing processes. This distinction is made by using a baroclinic stream function (the geopotential anomaly at 500 dbar relative to 1500 dbar, defined as $\phi_{500}^{1500} = \int_{500}^{1500} \delta dp$, where δ is the specific volume anomaly and p is pressure) as the cross-stream coordinate in place of geographical distance. Our results are insensitive to the exact choice of baroclinic stream function, because the ACC streamlines are equivalent barotropic and hence veer little with depth (Appendix A).

[15] The distance between ϕ_{500}^{1500} contours at each hydrographic section is computed as the mean distance between the contours averaged over all repeats of the section. We will refer to this pseudo-distance as Y, with the origin chosen as the southernmost station in the section. Since all sections are oriented approximately perpendicular to mean streamlines, Y is a reasonably good estimate of cross-stream distance. We opted for a definition of Y in terms of ϕ_{500}^{1500} (as opposed to sea level, which would give many more realizations than hydrographic section repeats) because we have greater confidence in the resolution of *in situ* cross-frontal variability in a geopotential anomaly-based reference frame rather than a sea level-based reference frame.

[16] After mapping the θ observations along all sections to a Y-γ^n grid, we calculate the θ_m distribution along each transect location by fitting a cubic spline to all the Y-θ data pairs sampled on each neutral surface. The choice of a cubic spline in this definition is motivated by the continuity of both the curve and its first derivative, which is implicated in the calculation of L_{mix} (see (3)). Any other smooth function with these properties gives very similar results to the ones presented here. An illustration of the calculation is provided by Figure 3. The θ_{rms} at location Y is estimated as the one standard deviation of $(\theta - \theta_m)$ for all measurements obtained within $Y \pm \Delta Y$. The thermal anomalies entering the calculation of θ_{rms} have characteristic vertical scales of O(10–100 m), comparable to the dimensions of cross-frontal interleaving features reported elsewhere [e.g., *Joyce et al.*, 1978; *Toole*, 1981]. The width of the interval ΔY is chosen to be in the range 30–150 km, with the exact value depending on the spatial density of sampling and the width of the ACC at each transect location. Our choice is guided by the requirement to have at least 5–10 data points in each calculation interval to approach statistical stability. This calculation of L_{mix} exhibits only minimal sensitivity to ΔY values on the order of 10–100 km (Appendix A). In essence, our definition of θ_m is identical to that of the gravest empirical mode of *Sun and Watts* [2001], while θ_{rms} measures the extent to which the observed θ departs from that modal structure.

[17] The distributions of θ_m arising from the preceding calculations are shown in Y-γ^n space for each of the five transect locations (Figures 4a, 5a, 6a, 7a, and 8a). The main water masses and frontal features of the Southern Ocean can be immediately recognized. A relatively warm ($\theta_m \sim$ 1–3°C)

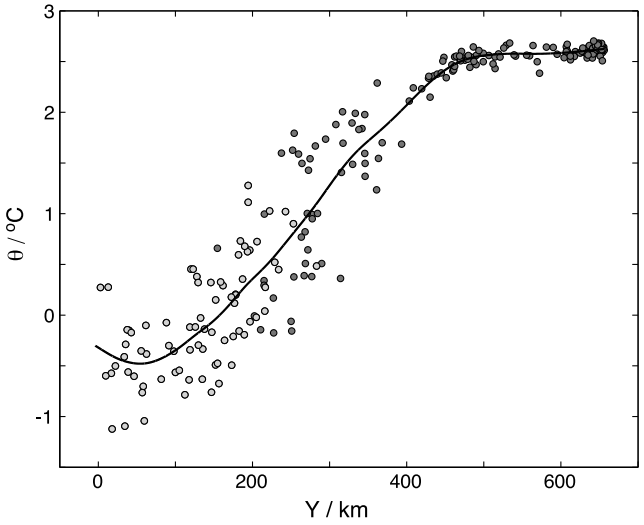

Figure 3. The θ measurements (shaded circles) on the 27.7 kg m^{-3} isoneutral as a function of along-transect pseudo-distance Y (defined in section 4.1) for ten occupations of the WOCE SR1b section in eastern Drake Passage. Light- (dark-) shaded circles indicate measurements at pressures smaller (larger) than 150 db, typical of the winter mixed layer base across much of the ACC. The cubic spline fit defining θ_m is shown by the solid line.

and voluminous body of CDW is seen to occupy the bulk of the sections at densities in excess of $\gamma^n \sim 27.6$ kg m^{-3}, overlying a layer of colder (θ_m 3 < 0°C) and denser ($\gamma^n >$ 28.27 kg m^{-3}) AABW near the southern end of the WOCE SR1b, I6S, I8S and SR3 transects. In the upper layers, a subsurface θ_m minimum colder than $\theta_m \sim 2$°C is observed in each of the sections to the south of the Polar Front, denoting the core of the wintertime variety of Antarctic Surface Water (referred to as Winter Water). Warmer ($\theta_m > 3$°C) upper-ocean waters are found further to the north. These indicate the presence of SAMW and AAIW equatorward of the Subantarctic Front, underlying a thin layer of surface waters.

[18] The cross-stream isoneutral gradient of θ_m at each of the transect locations is displayed in Figures 4b, 5b, 6b, 7b, and 8b. These reveal that the thermohaline gradients upon which eddies act are largest in the upper layers of the Polar Front (particularly in Drake Passage) and of the Subantarctic and Subtropical Fronts (in WOCE I6S, I8S and SR3), as well as more generally along the base of the pycnocline. The patterns in the distribution of θ_{rms} (Figures 4c, 5c, 6c, 7c, and 8c) broadly follow those in the $\nabla_n\theta_m$ field, indicating that the local rate of thermal variance production by eddy stirring along neutral surfaces is highly dependent on the local isoneutral gradient of θ_m. However, the covariation of θ_{rms} and $\nabla_n\theta_m$ is not perfect. Rather, it exhibits substantial spatial inhomogeneity, its structure reflecting variations in the mixing length scale L_{mix}.

[19] Estimates of L_{mix} as defined in (3) are shown in Figures 4d, 5d, 6d, 7d, and 8d. We estimate that L_{mix} varies by at least one order of magnitude. Values on the order of 5–10 km are commonly found in the upper layers (uppermost 500–1000 m) of the major ACC frontal jets, identified by their geostrophic velocity expressions in Figures 4e, 5e, 6e, 7e, and 8e, whereas mixing lengths of 50–150 km occur in the jets' deeper layers and in interfrontal regions. The finding that the mixing length scale inferred from isoneutral θ fluctuations is comparable to or smaller than the horizontal eddy length scale of O(100 km) lends further support to our interpretation of those fluctuations as being the product of eddy stirring (Appendix B).

[20] We find a notable suppression of L_{mix} in the four frontal jets in western Drake Passage (Figures 4d and 4e); the PF and SBdy in eastern Drake Passage (Figures 5d and 5e); the STF, SAF and SACCF in WOCE I6S (Figures 6d and 6e); the STF, SAF and PF in WOCE I8S (Figures 7d and 7e); and the SAF's southern branch, the two branches of the PF, SACCF and SBdy south of Tasmania (Figures 8d and 8e). Only in three frontal jet sites do we find an obvious absence of eddy mixing length suppression: the SAF in WOCE SR1b (Figures 5d and 5e), the PF south of Africa (Figures 6d and 6e), and the SAF's northern branch in WOCE SR3 (Figures 8d and 8e). The correspondence, or lack thereof, between areas of reduction in L_{mix} and fronts is ambiguous in a few of the weaker jets, namely the SACCF in eastern Drake Passage (Figures 5d and 5e), the SBdy in WOCE I6S (Figures 6d and 6e), and the SACCF and SBdy in WOCE I8S (Figures 7d and 7e). To summarize out of 24 frontal jet crossings, 17 exhibit evidence of suppression, such evidence is ambiguous in 4, and only 3 definite exceptions are noted.

[21] We note that the increased magnitude of L_{mix} in the deep ACC, below a depth of approximately 1000 m, is of dubious significance as it is associated with the tendency of $\nabla_n\theta_m$ toward zero there. This tendency could indeed reflect intense eddy stirring at depth, but it might also be a consequence of the general increase in the ventilation age of water masses with depth. In spite of this caveat, at least one piece of unambiguous evidence can be uncovered that points toward a genuine intensification of eddy stirring with depth at the ACC frontal jets. Such evidence may be found in the quasi-synoptic survey of the PF conducted during ISOS [*Joyce et al.*, 1978], which lies approximately 250 km to the east of the northern end of the WOCE S1 transect (Figure 2a) and was much more densely sampled than any WOCE section, thereby providing a unique view of the current's thermohaline structure. Using this data set, we construct a cross-frontal section with a variable horizontal resolution of 3–15 km. The distributions of θ_m, $\nabla_n\theta_m$, θ_{rms}, and L_{mix} in Y-γ^n space along this section are displayed in Figures 9a–9d and exhibit many of the properties that we encounter in the WOCE transects. The ISOS section spans across the northern flank of the PF, as denoted for example by the northern terminus of the Winter Water θ_m minimum at $\gamma^n \sim 27.45$ kg m^{-3} near $Y \sim 30$ km (Figure 9a). The strongest θ_m gradients are seen in waters lighter than $\gamma^n \sim$ 27.7 kg m^{-3} in the horizontal proximity of this terminus (Figure 9b), and occur in association with slightly elevated values of θ_{rms} (Figure 9c). It is in this area that eddy stirring is most strongly suppressed and L_{mix} values under 10 km are found (Figure 9d). These values are comparable to the cross-frontal length scales of the coherent interleaving features observed in the upper part of the PF during ISOS [*Toole*, 1981]. North of and below the upper layers of the front's northern flank, eddy stirring is no longer inhibited, and L_{mix} is typically an order of magnitude larger.

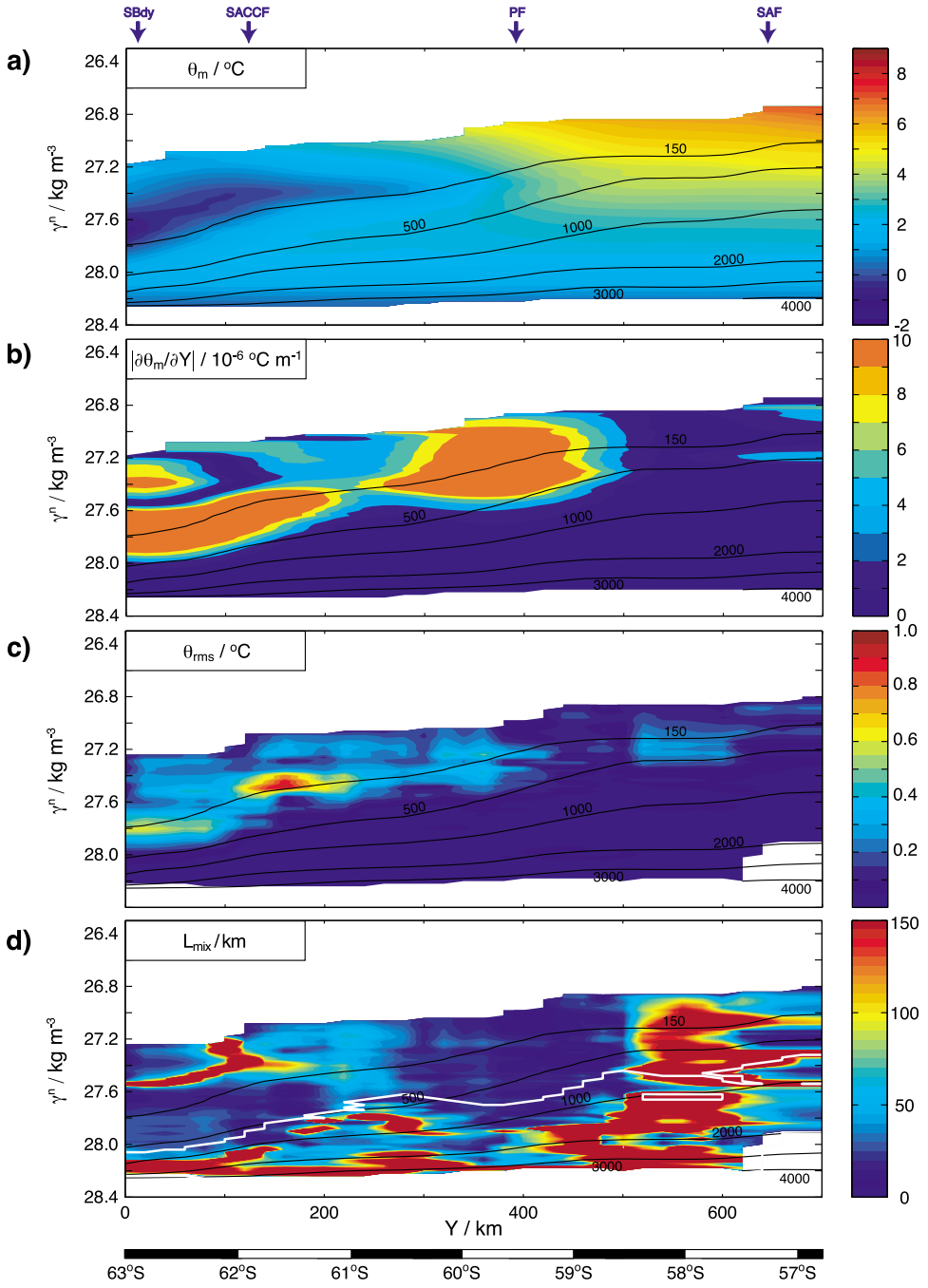

Figure 4. Distributions of (a) θ_m; (b) $\nabla_n\theta_m$; (c) θ_{rms}; (d) L_{mix}; (e) U_{geos}, the geostrophic velocity relative to the deepest common level; (f) U_e; (g) $c_e^{-1}\kappa$ and (h) the natural logarithm of (planetary) potential vorticity q, as a function of Y and γ^n along the WOCE S1 section. The black lines denote selected pressure contours, labeled in dbar. The white lines in Figures 4d and 4g show the upper boundary of the area of the deep Southern Ocean where $\nabla_n\theta_m \approx 0$, and so L_{mix} and $c_e^{-1}\kappa$ are ill-defined. The positions of hydrographic fronts are indicated at the top of each set of panels and labeled as in Figures 1 and 2. Frontal jets interpreted to exhibit (lack) mixing suppression in their upper and intermediate layers are labeled in blue (red), with ambiguous cases indicated in black. Our criterion for categorizing a jet as exhibiting (lacking) suppression is $\langle U_{geos}\rangle > 0.08$ m s^{-1}, $\langle L_{mix}\rangle < 50$ km ($\langle U_{geos}\rangle > 0.08$ m s^{-1}, $\langle L_{mix}\rangle > 100$ km), where angled brackets indicate an average over the part of the water column between the 150 db and 1000 db pressure contours.

[22] We now wish to direct the reader's attention to a feature in the ISOS section that was not immediately apparent in the WOCE transects: the boundary between the regions of weak and intense stirring in and north of the PF, respectively, is not vertical. Rather, it has a distinct slope of $O(5 \times 10^{-3})$ that broadly parallels geostrophic isotachs (Figure 9e). That the area of reduced stirring in the upper layers of the frontal jet is bowl-shaped and has sloping

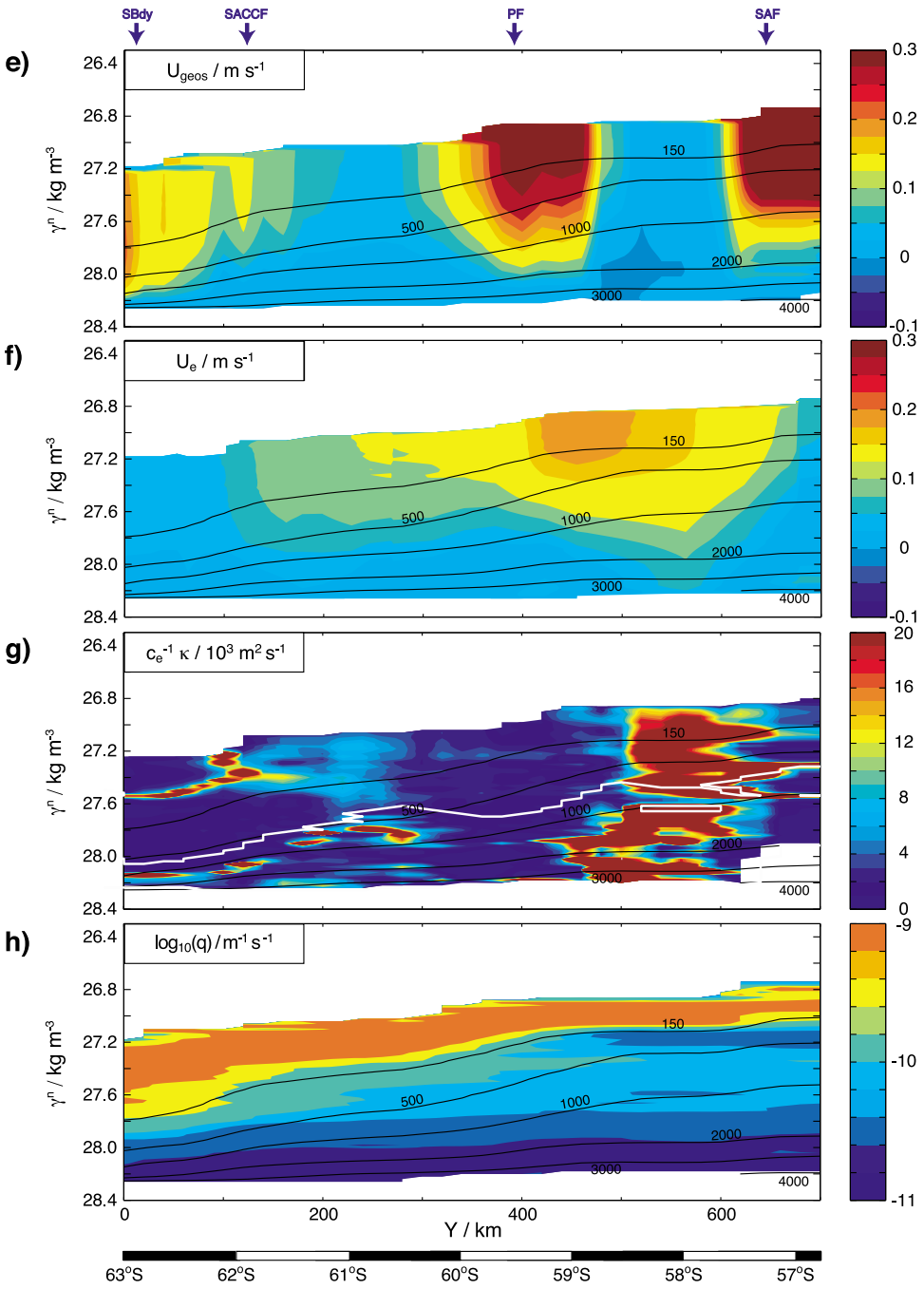

Figure 4. (continued)

lateral boundaries is further evidenced by the distribution of $\nabla_n^2\theta_m \approx \partial^2\ \theta_m/\partial Y^2$ along neutral surfaces in the ISOS section (Figure 9g). A band of markedly negative values occupies the deeper part of the region of weak stirring (Figure 9d) and mimics the shape of mean flow contours (Figure 9e). Equatorward of this band, $\partial^2\theta_m/\partial\ Y^2 \approx 0$, as would be expected from a region of strong stirring where any curvature in θ_m tends to be erased. We conclude that the detailed thermohaline structure of the PF in the ISOS section points to the existence of an inverse relationship between the mean flow speed and the eddy stirring rate, and is thus consistent with a genuine intensification of eddy stirring with depth at the ACC frontal jets.

3.2. Estimates of the Eddy Velocity U_e From Altimetry

[23] We estimate the cross-stream eddy velocity scale U_e as the one standard deviation in time of $\mathbf{u} \cdot \hat{\mathbf{n}}$, where $\mathbf{u}$ is the horizontal velocity vector, and $\hat{\mathbf{n}}$ is the unit vector perpendicular to the time-mean horizontal velocity $\overline{\mathbf{u}}$. The calculation consist of five steps. First, we construct a 15-year

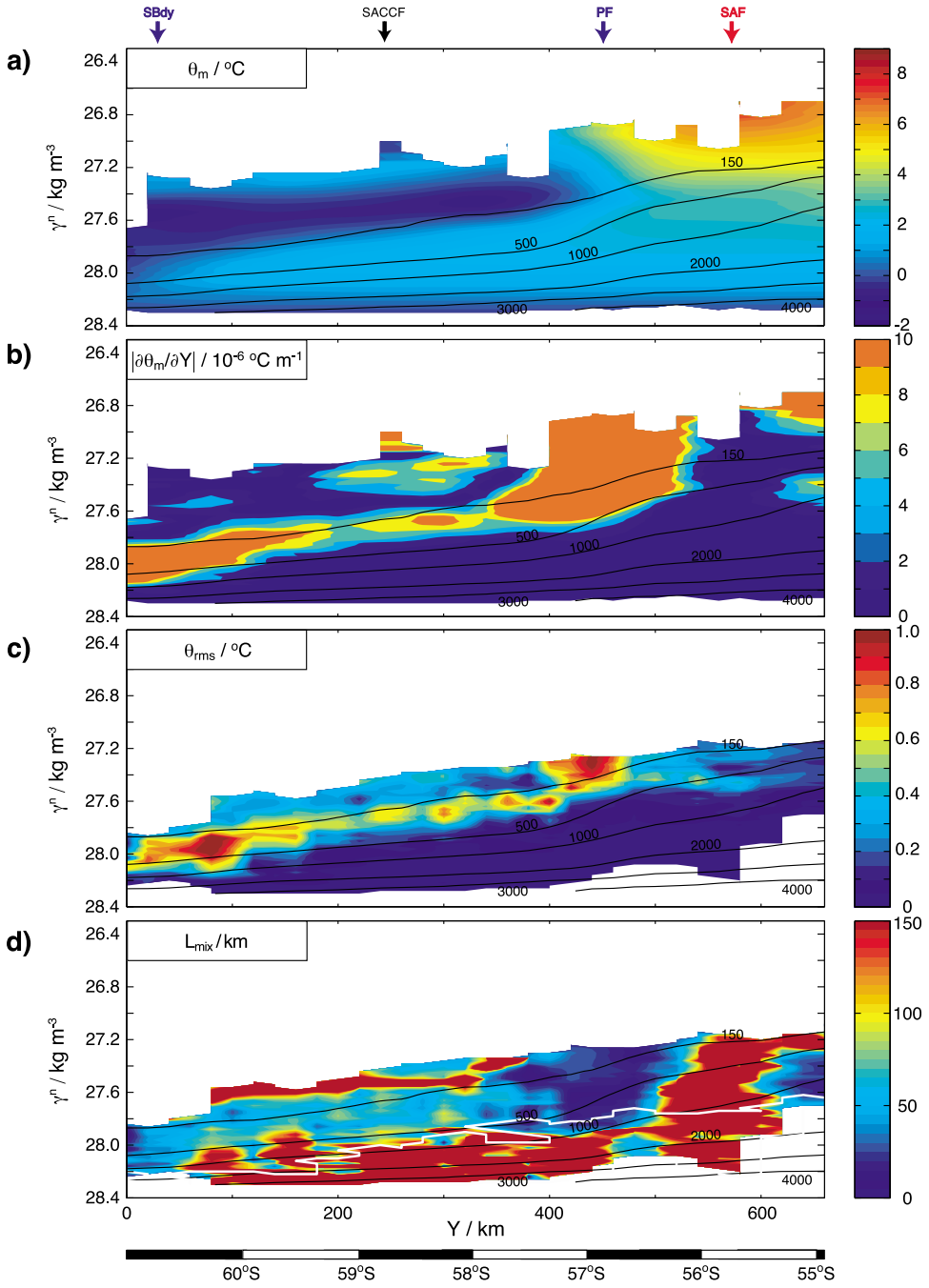

Figure 5. Distributions of (a) θ_m; (b) $\nabla_n\theta_m$; (c) θ_{rms}; (d) L_{mix}; (e) U_{geos}, the geostrophic velocity relative to the deepest common level; (f) U_e; (g) $c_e^{-1}\,\kappa$ and (h) the natural logarithm of (planetary) potential vorticity q, as a function of Y and γ^n along the WOCE SR1b section. The black lines denote selected pressure contours, labeled in dbar. The white lines in Figures 5d and 5g show the upper boundary of the area of the deep Southern Ocean where $\nabla_n\theta_m \approx 0$, and so L_{mix} and $c_e^{-1}\,\kappa$ are ill-defined. The positions of hydrographic fronts are indicated at the top of each set of panels and labeled as in Figures 1 and 2. Frontal jets interpreted to exhibit (lack) mixing suppression in their upper and intermediate layers are labeled in blue (red), with ambiguous cases indicated in black. Our criterion for categorizing a jet as exhibiting (lacking) suppression is given in the caption of Figure 4.

time series of weekly maps of sea surface height η by interpolating along each section the combined altimetric and absolute dynamic topography products introduced in Section 2. Second, along each transect, we map the γ^n and surface geopotential anomaly relative to an isobaric surface of pressure p, ϕ_0^p, as a function of η at the time of the transect and p. Then we fit cubic splines to the γ^n-η and ϕ_0^p-η pairs at each isobaric level. The procedure is analogous to the

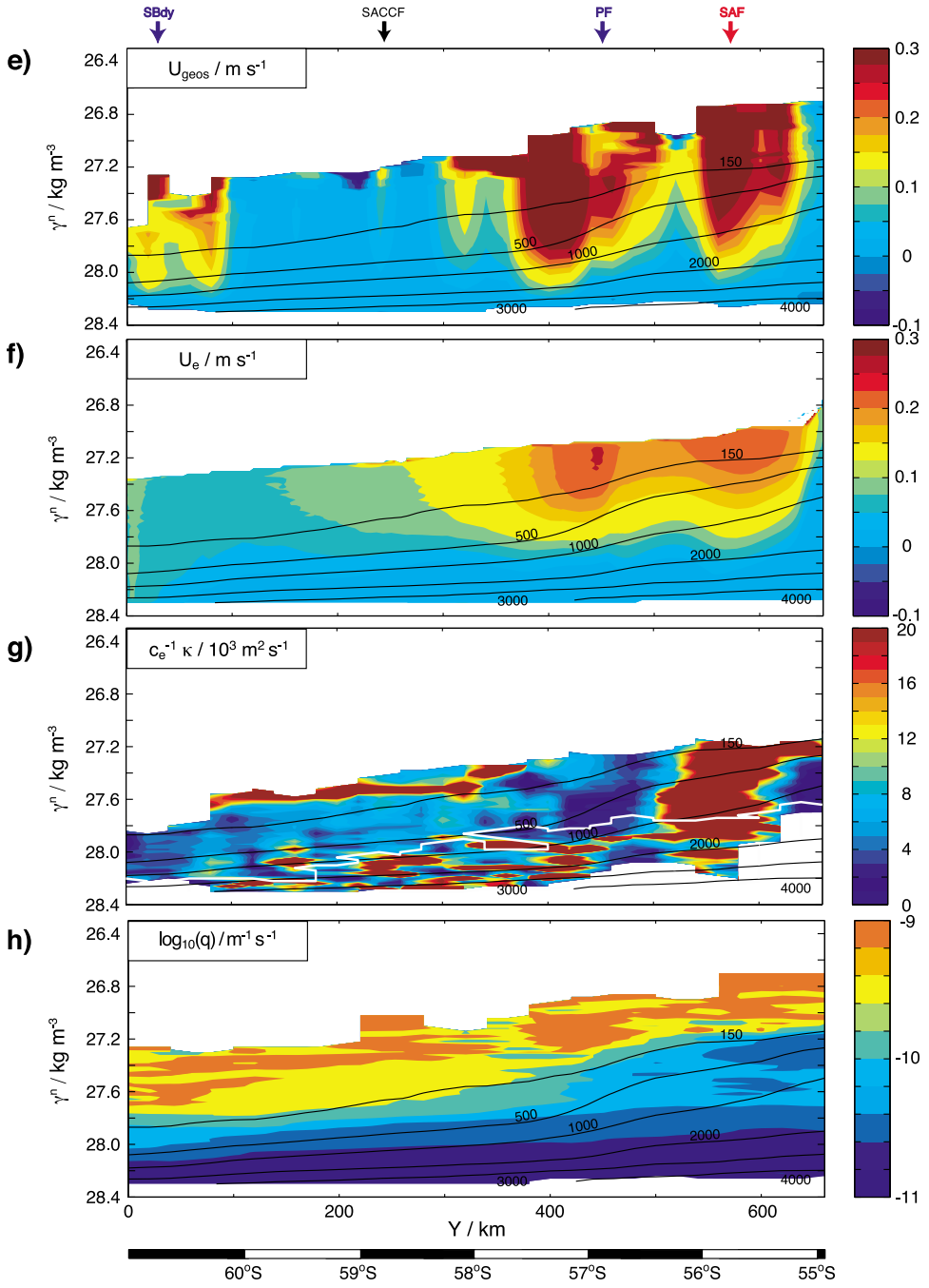

Figure 5. (continued)

gravest empirical mode calculation of *Sun and Watts* [2001]. Third, we use these sets of spline fits to obtain weekly, two-dimensional (i.e., as a function of η and p) estimates of the γ^n and **u** fields along each hydrographic section location. The surface **u** field is calculated from η using thermal wind, and projected to depth using ϕ_0^p-derived geostrophic shear. Fourth, we map the along-transect distribution of **u**, which is originally estimated on a pressure-based vertical grid, to the γ^n grid used in the calculation of L_{mix}. Fifth, we compute U_e (η, γ^n) from the expression above and use the mean (of all section repeats) profile of sea level (which is tightly related to ϕ_{500}^{1500}) versus along-transect distance for each section to obtain U_e (Y, γ^n), i.e., expressed in the same coordinates as L_{mix}.

[24] The resulting distributions of U_e along the sections are shown in Figures 4f, 5f, 6f, 7f, and 8f. These exhibit prominent maxima in a broad region around the SAF and PF, and secondary maxima near some of the other frontal jets. Minima in U_e are generally found near the current's poleward and equatorward edges. There is also a conspicuous decreasing tendency with depth that stems from the equivalent barotropicity of the ACC. All in all, the U_e distributions reflect the well-known patterns of EKE in the Southern Ocean (cf. Figure 2b), and imply the existence of

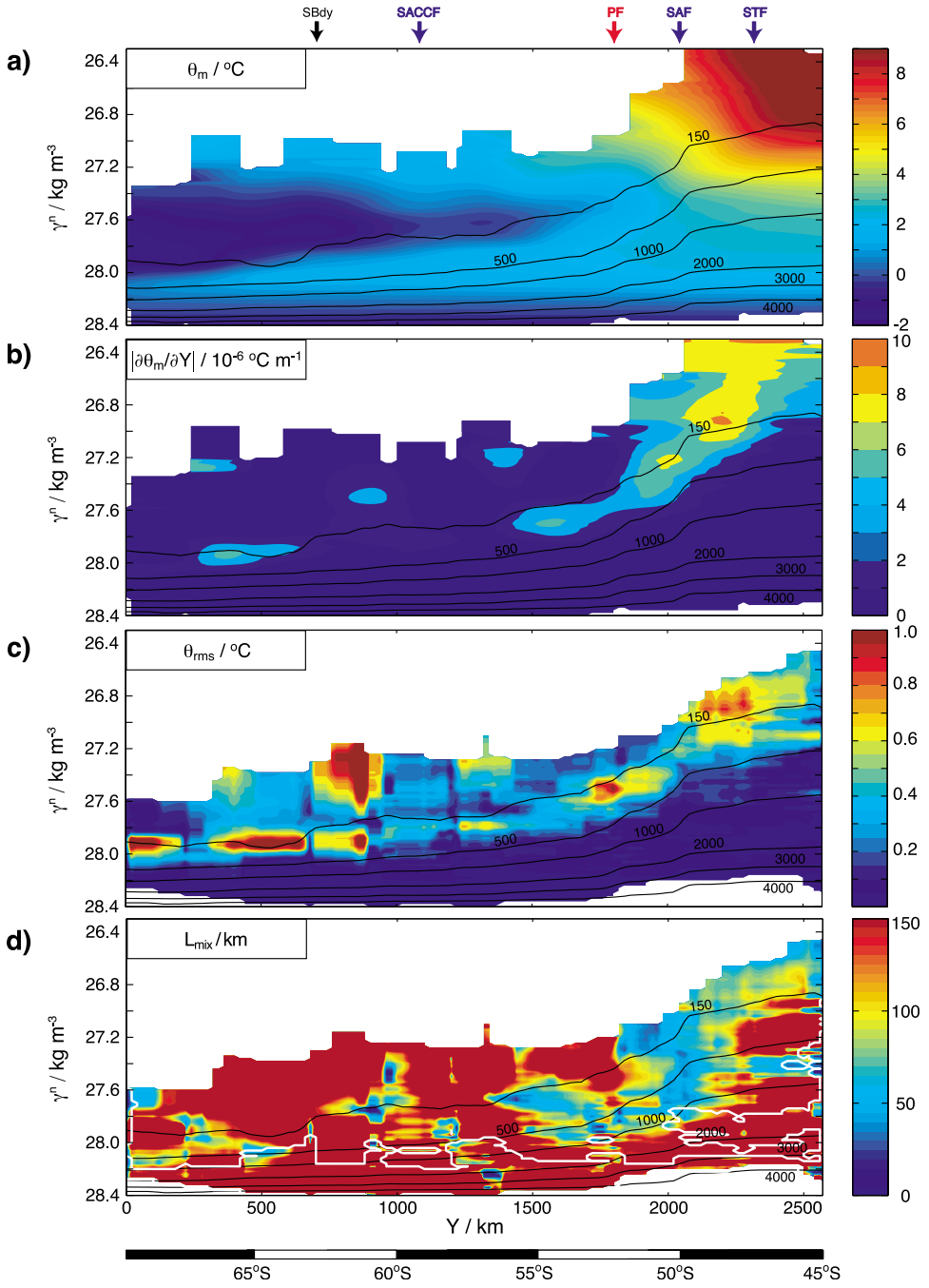

Figure 6. Distributions of (a) θ_m; (b) $\nabla_n\theta_m$; (c) θ_{rms}; (d) L_{mix}; (e) U_{geos}, the geostrophic velocity relative to the deepest common level; (f) U_e; (g) $c_e^{-1}\,\kappa$ and (h) the natural logarithm of (planetary) potential vorticity q, as a function of Y and γ^n along the WOCE I6S section. The black lines denote selected pressure contours, labeled in dbar. The white lines in Figures 6d and 6g show the upper boundary of the area of the deep Southern Ocean where $\nabla_n\theta_m \approx 0$, and so L_{mix} and $c_e^{-1}\,\kappa$ are ill-defined. The positions of hydrographic fronts are indicated at the top of each set of panels and labeled as in Figures 1 and 2. Frontal jets interpreted to exhibit (lack) mixing suppression in their upper and intermediate layers are labeled in blue (red), with ambiguous cases indicated in black. Our criterion for categorizing a jet as exhibiting (lacking) suppression is given in the caption of Figure 4.

a broad anticorrelation between the structure of the U_e and L_{mix} fields. Nonetheless, there are two notable differences between these fields. First, the characteristic lateral (along a neutral surface) width of U_e maxima is significantly larger (typically by a factor of ~2) than that of L_{mix} minima. Second, the range of variation in U_e across a front is substantially smaller than the range of variation in L_{mix} (a factor of 2–3 in U_e versus at least an order of magnitude

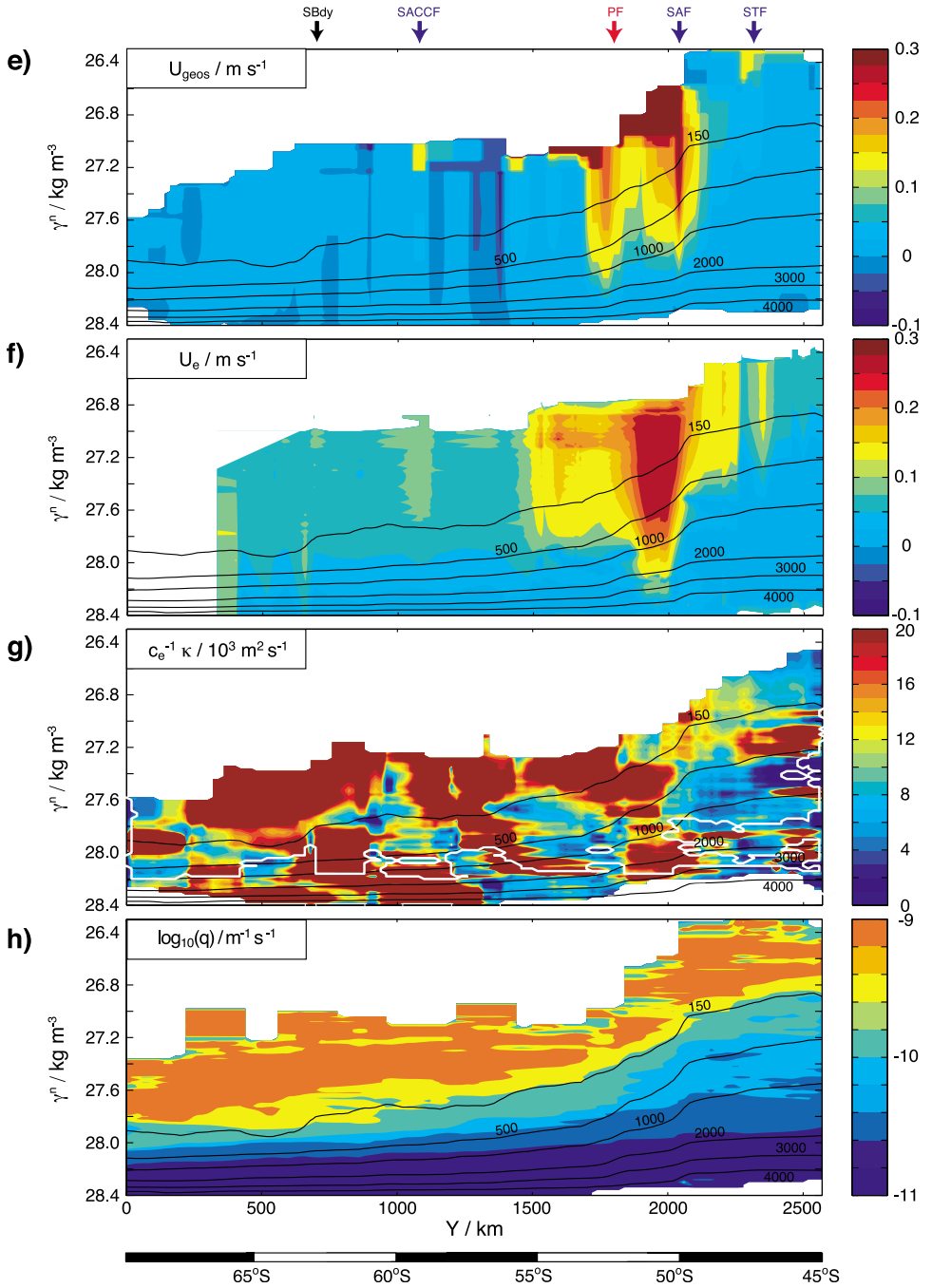

Figure 6. (continued)

in L_{mix}). Consequently, the structure of the L_{mix} field prevails over that of U_e in shaping the anatomy of κ in the Southern Ocean, although vertical variations in U_e cannot be neglected.

3.3. Estimates of the Isentropic Eddy Diffusivity κ

[25] The dominance of L_{mix} in determining κ is explicitly demonstrated by Figures 4g, 5g, 6g, 7g, and 8g, which show the distribution of U_e L_{mix} across each of the meridional sections analyzed here. We remind the reader that, in a mixing length theoretical framework (represented by (2)), U_e L_{mix} is equivalent to c_e^{-1} κ, where c_e is the supposedly constant mixing efficiency of eddies. We prefer to discuss c_e^{-1} κ rather than κ *per se* because of the uncertainty surrounding the magnitude of c_e. Estimates of c_e in the literature are based chiefly on the analysis of numerical simulations of a fully developed mesoscale eddy field [e.g., *Holloway and Kristmannsson*, 1984; *Visbeck et al.*, 1997; *Karsten et al.*, 2002], and generally fall in the range 0.01–0.4. This wide range likely reflects differences in the definition of L_{mix}. Many theoretical studies test the mixing length argument in terms of a length that scales with, but is not equal to, the mixing length scale proper (e.g., the eddy size). In these cases, c_e accounts for the relationship between

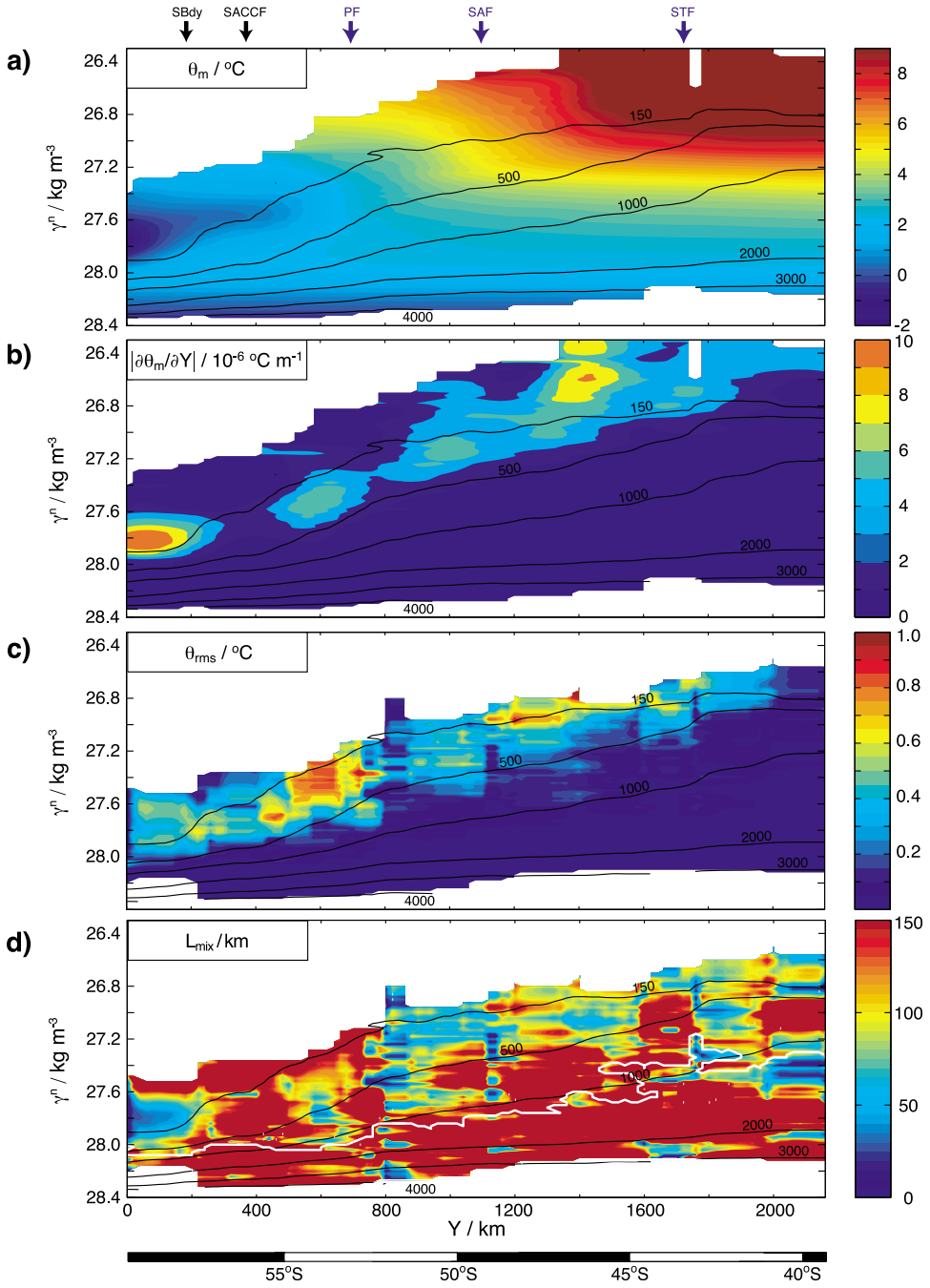

Figure 7. Distributions of (a) θ_m; (b) $\nabla_n\theta_m$; (c) θ_{rms}; (d) L_{mix}; (e) U_{geos}, the geostrophic velocity relative to the deepest common level; (f) U_e; (g) $c_e^{-1}\,\kappa$ and (h) the natural logarithm of (planetary) potential vorticity q, as a function of Y and γ^n along the WOCE I8S section. The black lines denote selected pressure contours, labeled in dbar. The white lines in Figures 7d and 7g show the upper boundary of the area of the deep Southern Ocean where $\nabla_n\theta_m \approx 0$, and so L_{mix} and $c_e^{-1}\,\kappa$ are ill-defined. The positions of hydrographic fronts are indicated at the top of each set of panels and labeled as in Figures 1 and 2. Frontal jets interpreted to exhibit (lack) mixing suppression in their upper and intermediate layers are labeled in blue (red), with ambiguous cases indicated in black. Our criterion for categorizing a jet as exhibiting (lacking) suppression is given in the caption of Figure 4.

U_e and the scale of choice. For illustrative purposes, we may use the only observational estimate of $c_e \approx 0.16$ obtained by *Wunsch* [1999] from the analysis of a quasi-global inventory of moored current meter and temperature records. Using this c_e value yields diffusivities of O(200 $m^2\ s^{-1}$) in the core of jets, and of O(2000 $m^2\ s^{-1}$) in inter-frontal regions. Regardless of which c_e value is adopted, Figures 4g, 5g, 6g, 7g, and 8g indicate that the structure of $c_e^{-1}\,\kappa$ is nearly identical to that of L_{mix}, at least in the upper ~1 km of the water column. At greater depth, the decrease in U_e becomes

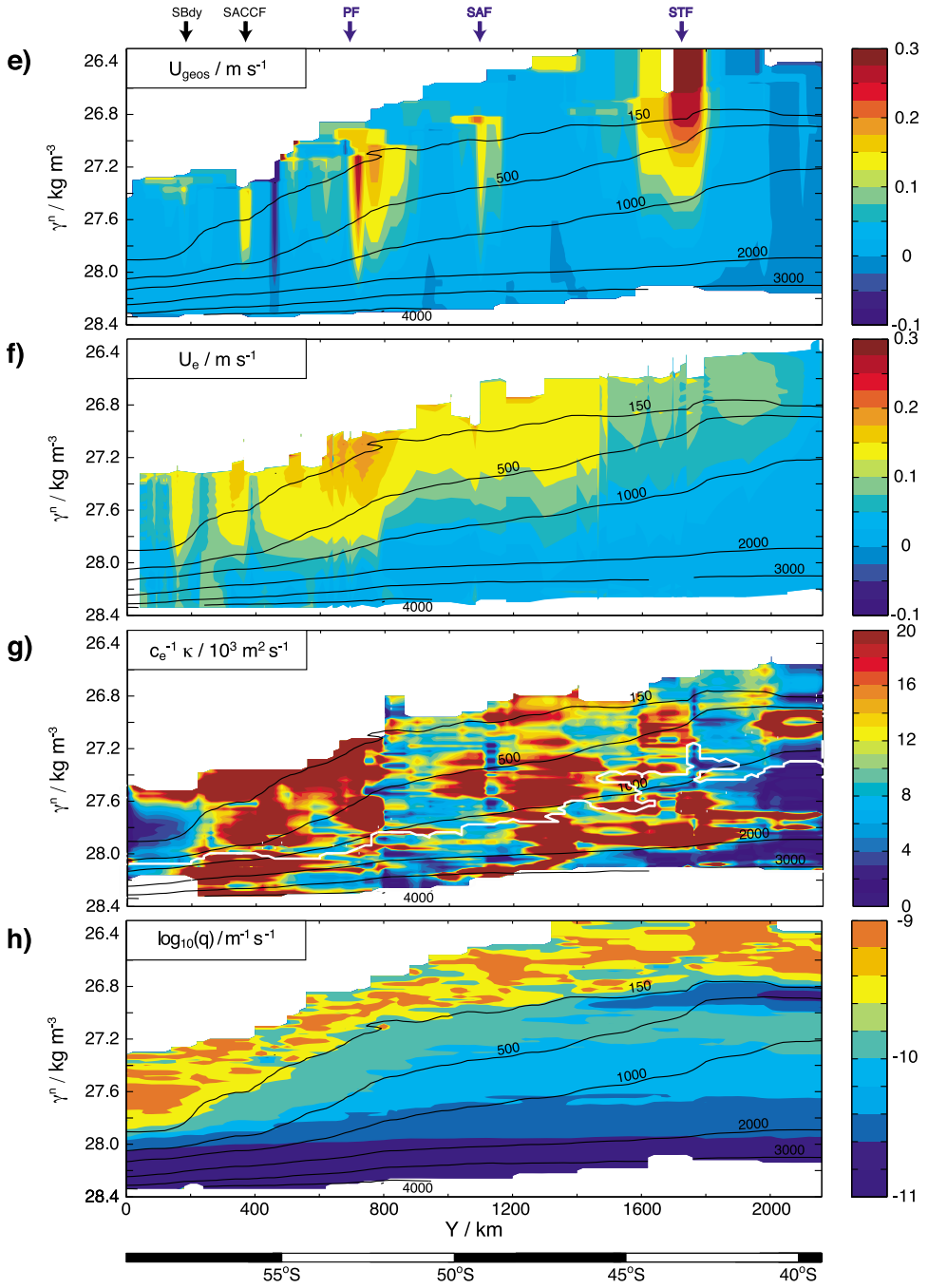

Figure 7. (continued)

significant, and $c_e^{-1}\ \kappa$ is often seen to decay toward the sea floor in a way that L_{mix} does not. The $c_e^{-1}\ \kappa$ distributions indicate that eddy stirring is regularly suppressed in the upper layers of the ACC frontal jets, and that it is intense in the deeper part of the jets and in interfrontal regions. We note that the area of mixing suppression associated with each jet often extends beyond the depth range of significant isentropic PV gradients (cf. Figures 4d, 5d, 6d, 7d, and 8d and Figures 4h, 5h, 6h, 7h, and 8h), as may be expected from a kinematic interpretation of the suppression.

[26] As in the analysis of L_{mix}, we find three unambiguous exceptions to the generalized reduction of eddy stirring at the core of the ACC frontal jets, with high values of $c_e^{-1}\ \kappa$ found in the upper part of the SAF in WOCE SR1b (Figure 5g), the PF south of Africa (Figure 6g), and the SAF's northern branch in WOCE SR3 (Figure 8g). In those sites, high diffusivities occur in conjunction with sizeable isentropic PV gradients (see Figures 5h, 6h, and 8h).

4. Discussion: Interpretation of the Structure of the Isentropic Eddy Diffusivity in the Southern Ocean

[27] In this section, we examine the degree of consistency between the properties of eddy stirring across the ACC indicated by the preceding analysis and a hierarchy of

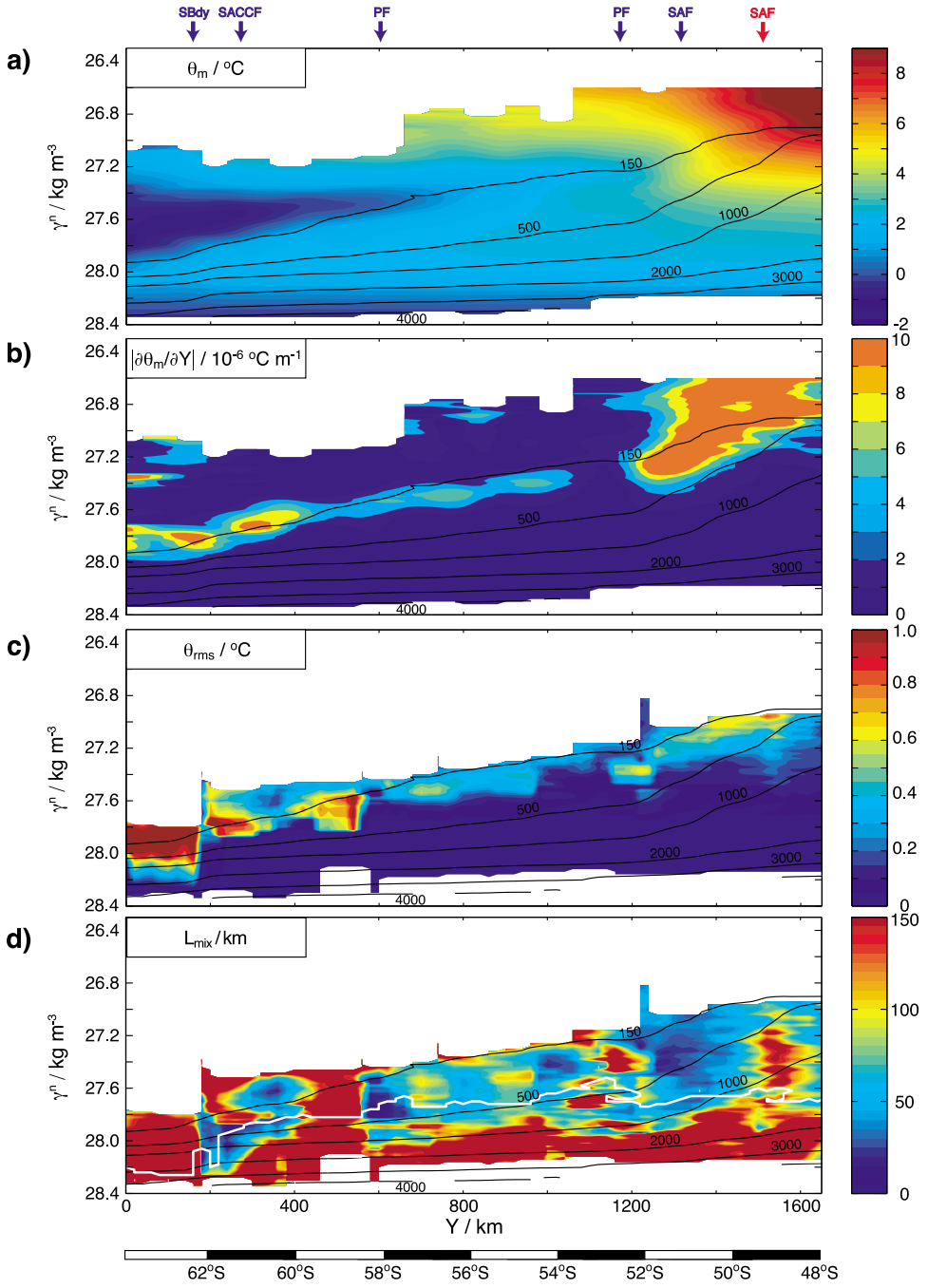

Figure 8. Distributions of (a) θ_m; (b) $\nabla_n\theta_m$; (c) θ_{rms}; (d) L_{mix}; (e) U_{geos}, the geostrophic velocity relative to the deepest common level; (f) U_e; (g) $c_e^{-1}\,\kappa$ and (h) the natural logarithm of (planetary) potential vorticity q, as a function of Y and γ^n along the WOCE SR3 section. The black lines denote selected pressure contours, labeled in dbar. The white lines in Figures 8d and 8g show the upper boundary of the area of the deep Southern Ocean where $\nabla_n\theta_m \approx 0$, and so L_{mix} and $c_e^{-1}\,\kappa$ are ill-defined. The positions of hydrographic fronts are indicated at the top of each set of panels and labeled as in Figures 1 and 2. Frontal jets interpreted to exhibit (lack) mixing suppression in their upper and intermediate layers are labeled in blue (red), with ambiguous cases indicated in black. Our criterion for categorizing a jet as exhibiting (lacking) suppression is given in the caption of Figure 4.

dynamical ideas put forward to characterize eddy stirring across geophysical jets in the literature. While this comparison is somewhat qualitative, the theoretical ideas put to the test here yield such a wide range of predictions on the structure of eddy stirring that our observational results are well suited to discriminating between them. The most important observed characteristics of eddy stirring to be interpreted through a theoretical lens are synthesized by

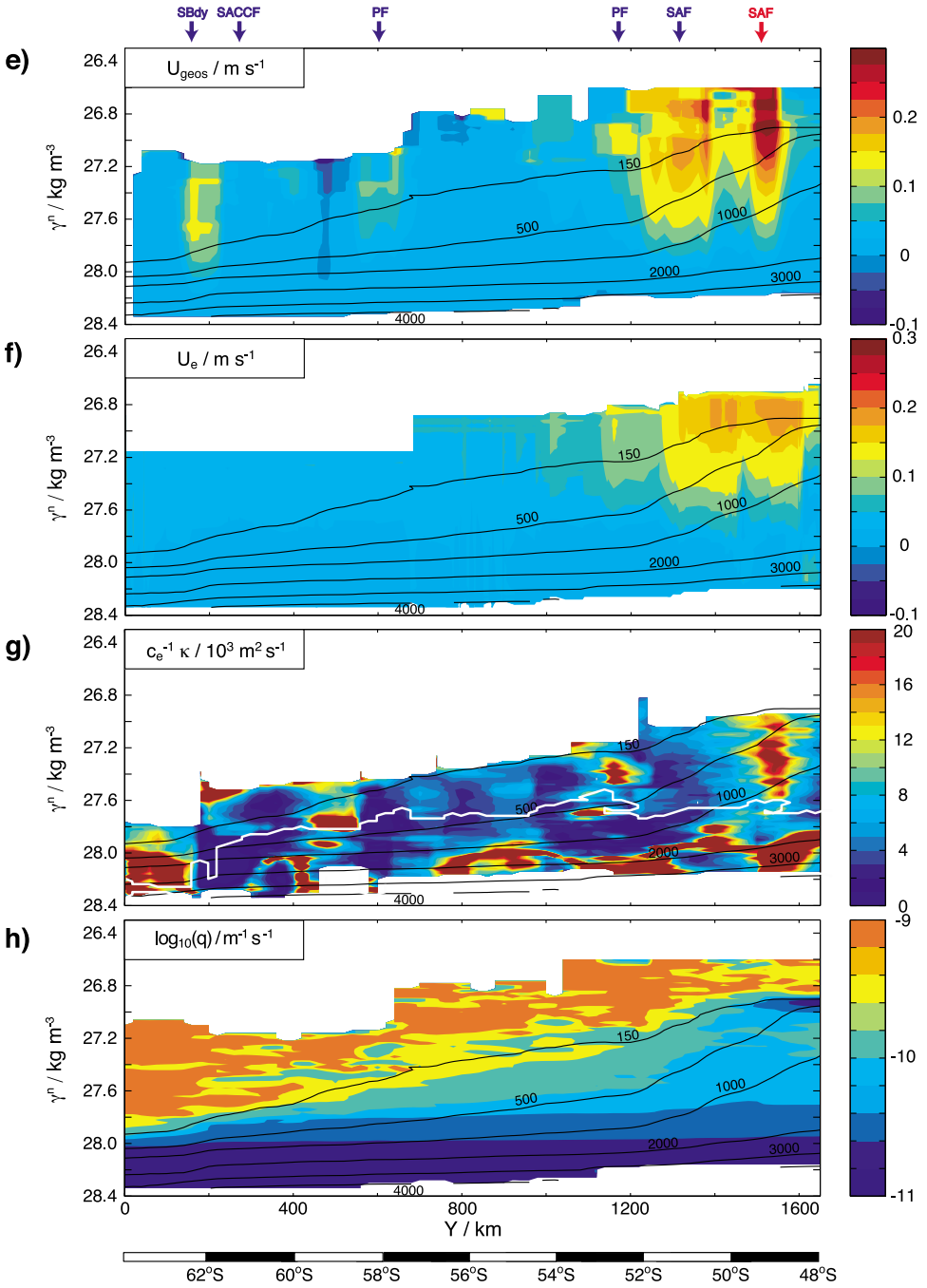

Figure 8. (continued)

Figure 10, in which estimates of L_{mix} across the entire data set analyzed here are averaged in bins of mean flow speed and displayed by colored symbols, with shading indicating U_e. Two groups of results are shown: averages over the three leaky jet regions identified above (squares), and averages over the remainder of the data set (circles). The regular eddy stirring properties in the ACC are represented by the latter group, for which L_{mix} is seen to decrease by an order of magnitude with increasing mean flow speed, despite a concurrent marked increase in U_e (or EKE). The former group illustrates a relatively rare but pronounced deviation from the norm: L_{mix} generally increases with increasing mean flow speed and U_e. Similar qualitative inferences may be drawn from the distribution of κ with respect to the mean flow speed and U_e (not shown).

[28] The theoretical ideas against which the key characteristics encapsulated in Figure 10 are to be interpreted include descriptions of eddy stirring as quasi-homogeneous turbulence (section 4.1), linear waves in a parallel shear flow (section 4.2),weakly nonlinear waves in a parallel shear flow (section 4.3), aspects of wave propagation in non-parallel shear flows (section 4.4), and near-boundary turbulent suppression (section 4.5). Such theoretical considerations lead, in brief, to predictions of enhanced eddy

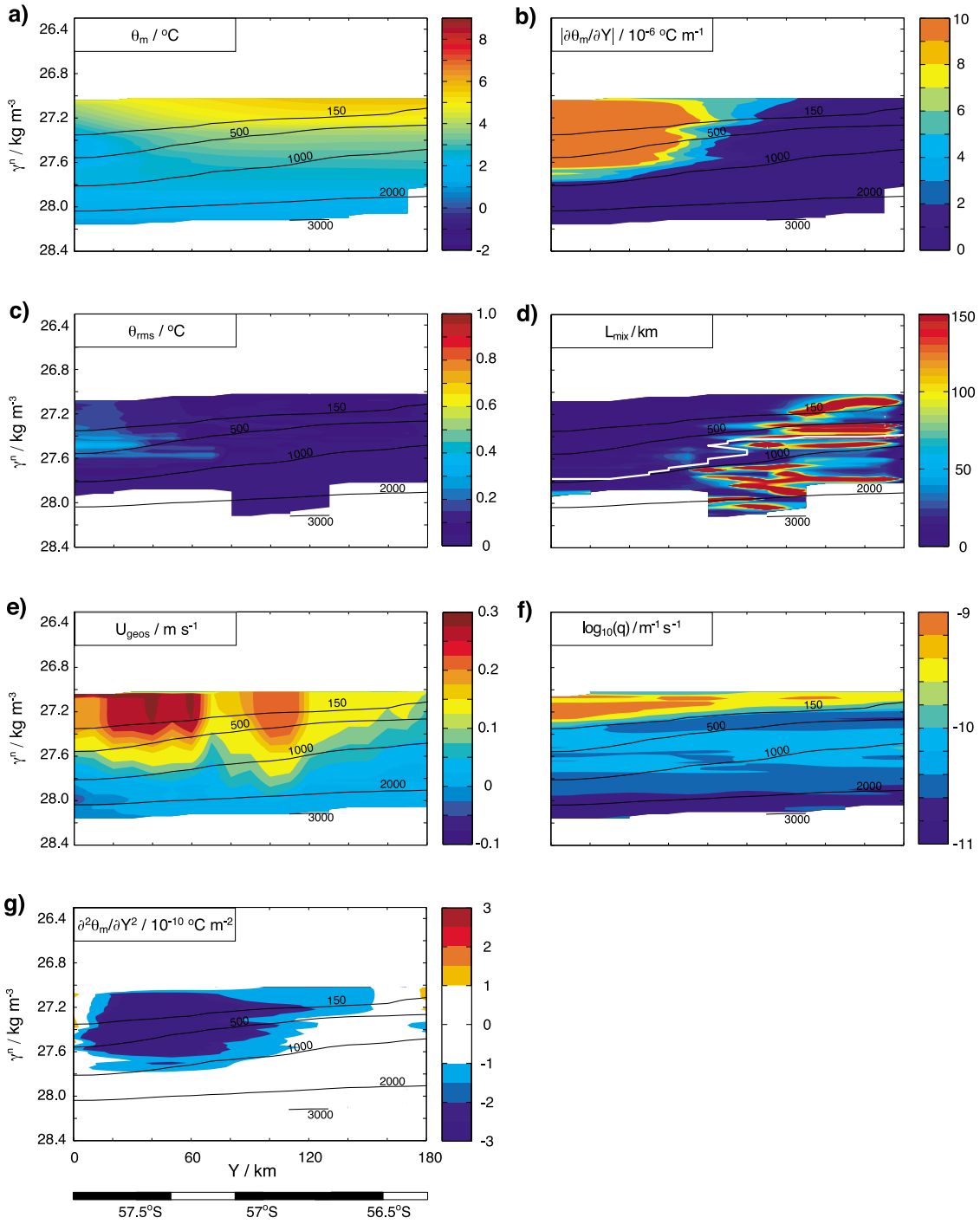

Figure 9. Distributions of (a) θ_m; (b) $\nabla_n\theta_m$; (c) θ_{rms}; (d) L_{mix}; (e) U_{geos}, the geostrophic velocity relative to the deepest common level; (f) $\log_{10}(q)$ and (g) $\partial^2\theta_m/\partial Y^2$, as a function of Y and γ^n along the ISOS section. The black lines denote selected pressure contours, labeled in dbar. The white line in Figure 9d shows the upper boundary of the area where $\nabla_n\theta_m \approx 0$ and L_{mix} is ill-defined.

stirring in jet cores (quasi-homogeneous turbulence), enhanced eddy stirring on jet flanks and below jet cores (linear waves in a parallel shear flow), suppressed eddy stirring in jet cores (weakly nonlinear waves in a parallel shear flow), potential breakdown of eddy stirring suppression in jet cores (aspects of wave propagation in non-parallel shear flows), and suppression of eddy stirring near a topographic boundary (near-boundary turbulent suppression). The key predictions, successes and failures relative to our observational results of each of these theoretical descriptions of eddy stirring are synthesized in Table 2, and expanded on in the remainder of this section. Our main conclusion is that the generalized reduction of L_{mix} and κ at the core of the ACC frontal jets present in our results are

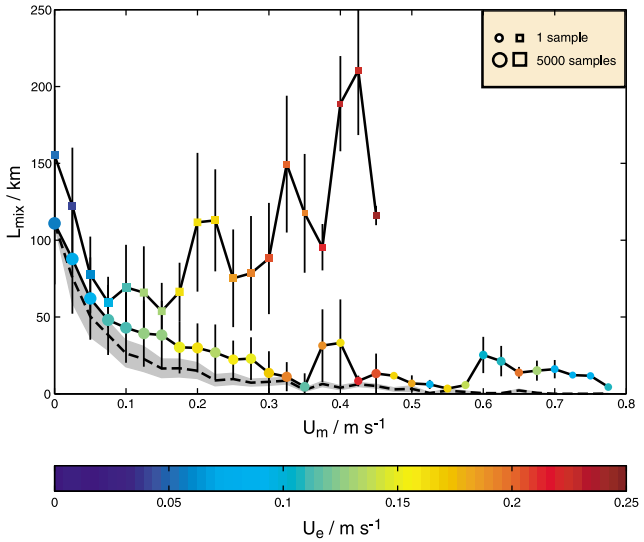

Figure 10. L_{mix} estimates (colored symbols, shaded by the average U_e) from the five sections analyzed here, averaged in bins of mean flow speed U_m. Squares show averages of L_{mix} estimates from the three leaky jet regions identified in section 3 (the SAF in WOCE SR1b, the PF south of Africa and the SAF's northern branch south of Tasmania). Circles show averages of L_{mix} estimates from the remainder of the sections. L_{mix} values greater than 700 km (mostly below 2000 m) or from the uppermost 100 m of the water column are disregarded in the averaging. The size of each symbol denotes the number of individual L_{mix} estimates contributing to the average value (see inset), and the vertical lines the standard deviation of individual L_{mix} estimates in each U_m bin. The dashed line shows the decay of L_{mix} with increasing U_m predicted by the inverse stirring suppression factor $(1 + 4U_m^2 EKE^{-1})^{-1}$ in (10), using the observed L_{mix} value at $U_m = 0$, the relation $EKE = U_e^2$, and the average U_e value in each U_m bin. The grey shading indicates the range of predicted L_{mix} values associated with one standard deviation of the individual estimates of U_e in each U_m bin.

best interpreted as a suppression of stirring by eddy interaction with parallel jets (as in section 4.3), and that the observed occasional deviations from this regime (the occurrence of three leaky jets) might plausibly be explained in terms of eddy interaction with narrow and twisted jets (as in section 4.4).

4.1. Eddy Stirring as Quasi-Homogeneous Turbulence

4.1.1. Concept

[29] Descriptions of eddy stirring as quasi-homogeneous turbulence date back to the classical work of *Taylor* [1921], who demonstrated that particle dispersion in a homogeneous, isotropic turbulent field implies an eddy diffusivity proportional to the product of the EKE and the eddy decorrelation time scale γ^{-1}, i.e.,

$$\kappa_{Taylor} \propto EKE\gamma^{-1}. \quad (4)$$

Considering that $U_e \propto EKE^{1/2}$, this result implies that the eddy mixing length scale in a turbulent field is given by $L_{mix} \propto EKE^{1/2}\ \gamma^{-1}$, which recovers the L_{mix}-based expression for the eddy diffusivity (2).

[30] Expressions of the form of (4) are often used to estimate eddy diffusivities in the ocean. Note, however, that estimates of γ are notoriously difficult to obtain because they require long-time Lagrangian observations. Lacking these, κ is expressed in terms of estimates of U_e and L_{mix}. It is typically argued that L_{mix} scales with the size of geostrophic eddies, thereby varying only gently in space, and hence κ depends primarily on EKE and is highest near the surface and in the core of jets. This point of view is put forward by, for example, *Holloway* [1986], *Keffer and Holloway* [1988], *Visbeck et al.* [1997] and *Stammer* [1998], who combine a variety of theoretical ideas on the characteristics of eddies [*Green*, 1970; *Stone*, 1972; *Holloway and Kristmannsson*, 1984; *Held and Larichev*, 1996] with satellite altimetric measurements and eddy-resolving numerical simulations to contend that surface κ is routinely enhanced in the core of the main ocean currents.

[31] The ideas stemming from this body of work find qualitative support in estimates of near-surface κ obtained from the application of Taylor's theory (4) to drifter data, which point to an enhancement of κ within the ACC core relative to surrounding regions and to a prevalence of U_e in shaping the lateral variability in surface κ [*Schäfer and Krauss*, 1995; *Sallée et al.*, 2008]. A quantification of surface eddy stirring based on finite-time Lyapunov exponents calculated from altimetric measurements yields similar findings [*Waugh and Abraham*, 2008]. In regard of

Table 2. Summary of Key Predictions, Successes and Failures, Relative to the Observational Findings of This Study, of the Theoretical Descriptions of Eddy Stirring Under Consideration

Theoretical Description	Key Predictions	Successes	Failures
Quasi-homogeneous turbulence	L_{mix} proportional to eddy size κ proportional to EKE	None	Widespread disagreement with observations
Linear waves	L_{mix} and κ enhanced at Rossby wave critical layers	L_{mix} and κ generally elevated at jet flanks relative to jet cores	No evidence of L_{mix} and κ enhancement at jet flanks relative to off-jet regions
Weakly nonlinear waves	L_{mix} and κ reduced by mean flow	L_{mix} and κ generally reduced in jets relative to surroundings	Three jets with high L_{mix} and κ
Eddy interaction with nonparallel mean flow	L_{mix} and κ not reduced by mean flow	Three jets with high L_{mix} and κ show some evidence of nonparallel conditions	SAF jet near South America shows nonparallel conditions yet reduced L_{mix} and κ
Near-boundary turbulent suppression	L_{mix} and κ reduced close to a solid boundary	SAF jet near South America shows nonparallel conditions yet reduced L_{mix} and κ	None

the vertical distribution, *Ferreira et al.* [2005] and *Olbers and Visbeck* [2005] report a surface intensification of the diffusivity and an exponential decay with depth based on various combinations of models and hydrography. Such a vertical decay would appear to be consistent with a reduction in EKE, and hence U_e, with depth. Note, though, that these latter estimates pertain to the diffusivity of buoyancy and should not be compared directly to the isopycnal diffusivity considered here (see, e.g., *Smith and Marshall* [2009] for a discussion of the relationship between the two types of diffusivity).

4.1.2. Assessment

[32] The assumption that L_{mix} is proportional to the size of geostrophic eddies and the ensuing result that the structure of κ is primarily determined by U_e are both inconsistent with our findings. These indicate that L_{mix} generally exhibits a marked reduction at the core of jets relative to their surroundings, and that it is the main variable shaping the κ distribution.

4.2. Eddy Stirring as Linear Waves

4.2.1. Concept

[33] An alternative description of eddy stirring in the Southern Ocean in terms of linear Rossby waves is provided by *Marshall et al.* [2006] who, in applying the 'effective diffusivity' technique of *Nakamura* [1996] to altimetric observations, suggest that surface κ values are amplified on the equatorward flank of the ACC relative to the current's axis, i.e., largely outside the region of highest EKE. This pattern is reminiscent of observations of eddy stirring in the atmosphere, where the intensification of mixing along jet flanks is thought to be associated with Rossby wave critical layers [e.g., *Haynes and Shuckburgh*, 2000a, 2000b], and is seemingly better aligned with the definition of jets as PV jumps in the geophysical literature [e.g., *Dritschel and McIntyre*, 2008].

[34] Critical layers arise in linear wave equations when the mean flow is considered. For our purpose, the lowest order incarnation of this type of equation is the barotropic quasi-geostrophic PV equation for linear eddy perturbations embedded in a large-scale and slowly-evolving zonal mean flow of speed U_m,

$$\partial_t q' + U_m \partial_x q' + \partial_x \psi' \partial_y \overline{q} = 0, \tag{5}$$

where ψ' denotes the eddy geostrophic stream function and $q' = \nabla^2 \psi'$ the eddy PV. With an assumption about the functional representation of $\overline{q}(y, z)$, and consequently $U_m(y, z)$, plane wave solutions to (5) of the form $\psi' \propto e^{i(kx-\sigma t)}$ exhibit large-amplitude cross-frontal displacements at critical layers with $U_m - c = 0$, where $c = \sigma/k$ is the phase speed of the wave, σ its intrinsic frequency, and k its zonal wavenumber [e.g., *Pratt et al.*, 1995]. Such large amplitudes imply markedly enhanced stirring rates relative to near-zero background values. In the linear wave limit, cross-jet mixing is absent away from critical layers.

[35] This characterization of eddy stirring is consonant with the linear instability theory of *Killworth* [1997] and the arguments of *Treguier* [1999], *Cerovečki et al.* [2009], *Smith and Marshall* [2009] and *Abernathy et al.* [2009] based on numerical simulations of varying complexity. These studies point to an enhancement of κ at depth, allegedly associated with Rossby wave critical layers. It has also been suggested that the critical layer phenomenon may underlie the observation of inhibited (intensified) exchange of floats in the upper ocean (at mid depth) across the Gulf Stream jet [*Bower et al.*, 1985; *Bower and Rossby*, 1989; *Bower and Lozier*, 1994; *Lozier et al.*, 1997; *Rogerson et al.*, 1999].

4.2.2. Assessment

[36] The results of our analysis in section 3 bear much qualitative resemblance to the preceding description of eddy stirring in terms of linear wave ideas, in that they indicate that κ does not depend strongly on EKE, and that stirring rates are enhanced outside of, rather than within, jet cores. However, a subtle discrepancy between our results and the linear wave interpretation is that we find no clear evidence of an enhancement of stirring rates in the upper ocean along jet flanks and at mid depth below jet cores relative to off-jet regions. Rather, L_{mix} and κ values in off-jet regions are comparable in magnitude to values enveloping jet cores.

4.3. Eddy Stirring as Weakly Nonlinear Waves

4.3.1. Concept

[37] A description of eddy stirring as weakly nonlinear waves is put forward by *Ferrari and Nikurashin* [2010], who investigate eddy stirring in a baroclinic quasi-geostrophic model. Their key result may be captured by considering the simpler problem of eddy-induced stirring across a barotropic jet. The barotropic quasi-geostrophic PV equation for weakly nonlinear eddy perturbations embedded in a large-scale and slowly-evolving zonal mean flow (cf. expression (5)) is given by

$$\partial_t q' + U_m \partial_x q' + \partial_x \psi' \partial_y \overline{q} + J(\psi', q') = 0, \tag{6}$$

where J the Jacobian operator. For simplicity, we assume that the mean flow is zonal. Curvature terms associated with bending of the mean flow are neglected, consistent with the assumption that the mean flow varies on scales much larger than the eddies.

[38] As with *Ferrari and Nikurashin* [2010], the nonlinear term $J(\psi, q)$ is represented with a fluctuation-dissipation stochastic model [*Landahl*, 1975; *Farrell and Ioannou*, 1993; *Flierl and McGillicuddy*, 2002]. The stochastic model is monochromatic to keep the problem linear and can be thought of as representing the excitation of waves by instability at horizontal wavenumber (k, l). Dissipation in a fluctuation-dissipation model is through linear damping at a rate γ which sets the eddy decorrelation time scale as shown below.

[39] The stream function solution of the stochastic model (see *Ferrari and Nikurashin* [2010] for details of the derivation) can be used to advect a tracer and compute the mixing length defined as the typical length of the resulting tracer filaments,

$$L_{mix} = \frac{k^2}{k^2 + l^2} \frac{EKE^{1/2}\gamma^{-1}}{1 + \gamma^{-2}k^2(U_m - c)^2}, \tag{7}$$

where $c = U_m - \partial_y \overline{q}/(k^2 + l^2)$ is the phase speed of barotropic Rossby waves propagating in the mean flow, and γ^{-1}

the eddy decorrelation (damping) time scale. Using (2), the reduction in L_{mix} results in a suppression of the eddy diffusivity,

$$\kappa \propto U_e L_{mix} = \frac{EKE\gamma^{-1}}{1+\gamma^{-2}k^2(U_m-c)^2}. \quad (8)$$

This expression synthesizes the key result of a characterization of eddy stirring in terms of weakly nonlinear waves. It suggests that the mixing length is proportional to the mean displacement induced by an eddy, $EKE^{1/2}\ \gamma^{-1}$, but also that the presence of a mean flow acts to reduce L_{mix}. Thus, for eddies propagating at the same speed as the jet, $c = U_m$, $L_{mix} \propto EKE^{1/2}\gamma^{-1}$ and the mean flow has no effect on mixing. However, when the eddy phase speed does not match the jet velocity, eddy propagation relative to the mean flow results in a temporal oscillation of cross-frontal displacements. If the oscillation period $k^{-1}\ (U_m - c)^{-1}$ is shorter than the eddy decorrelation time scale γ^{-1}, cross-frontal filamentation is arrested. This mixing length suppression is captured by the denominator in (7), which is proportional to the ratio of the advective and decorrelation time scales, and is purely a kinematic effect of coherent phase propagation.

[40] The eddy stirring suppression due to the presence of a mean flow is brought out most clearly by formulating the eddy diffusivity in (8) as a modification to Taylor's expression,

$$\kappa = \frac{\kappa_{Taylor}}{1+\gamma^{-2}k^2(U_m-c)^2}, \quad (9)$$

where $\kappa_{Taylor} = k^2\ (k^2 + l^2)^{-1}\ EKE\ \gamma^{-1}$ is Taylor's definition of the cross-jet (meridional) eddy diffusivity. The expression in (9) predicts that the diffusivity is reduced in the core of (broad) jets relative to the jets' flanks, as long as $U_m \geq c$ as is the case near strong ocean jets.

[41] It is important to note that, despite qualitatively endorsing the basic characterization of oceanic jet cores as mixing barriers, the expressions for κ in (8)–(9) differ in a significant way from the bulk of the oceanographic literature advocating that description. This literature [e.g., *Marshall et al.*, 2006; *Smith and Marshall*, 2009; *Abernathy et al.*, 2009] explains the spatial distribution of κ in the vicinity of a jet in terms of an enhancement of mixing at critical layers girdling the jet core. This stems from the widely accepted paradigm in the atmospheric community [e.g., *Randel and Held*, 1991] that eddies are linear waves with an infinite decorrelation time scale. In the limit $\gamma \to \infty$, κ vanishes everywhere (since κ_{Taylor} is proportional to γ^{-1}) except at critical lines. Mixing is therefore confined to critical lines. A generalization of this concept is the mixing in critical layers predicted by the chaotic mixing literature studying weakly nonlinear eddy fields [e.g., *Pierrehumbert*, 1991; *Rypina et al.*, 2007]. In the ocean, however, eddies are nonlinear [e.g., *Scott and Wang*, 2005; *Chelton et al.*, 2007], interact and thus have a finite decorrelation time scale. Indeed, we expect eddies to mix even in the absence of a mean flow, and hence in the absence of critical layers. Once a finite eddy decorrelation time scale is introduced in the problem, the mean flow acts to suppress mixing, and critical layers are simply regions where no suppression is observed.

4.3.2. Assessment

[42] Similarly to the linear wave case, the characterization of eddy stirring as weakly nonlinear eddies successfully reproduces the most prominent features of our observational results, namely that κ scales primarily with L_{mix} and that stirring rates are reduced within jets. Additionally, this description of eddy stirring is also consistent with the absence of obvious critical layer signatures in our diagnosed L_{mix} and κ distributions (i.e., the values of these two variables are comparable in the low-velocity envelopes of jet cores and in off-jet regions). This suggests that the weakly nonlinear eddy theory provides the more faithful characterization of the observations. In the following, we present further observational evidence in support of this interpretation.

[43] The emerging picture of widespread mixing suppression along the ACC jets is suggestively endorsed by observations of the propagation of coherent eddy features in the ACC. *Hughes et al.* [1998] applied a Radon transform technique to altimetric measurements to estimate the zonal phase speeds of these eddying motions. An updated illustration (courtesy of C. Hughes, personal communication, 2009; a description of the calculation is given by *Smith and Marshall* [2009]) of their most fundamental result is shown in Figure 2d, where the observed zonal speed of eddy propagation is displayed along with mean dynamic topography. Zonal phase speeds are positive (eastward) in a broad band following the path of the ACC, whereas they are negative (westward) elsewhere, as expected from Rossby wave propagation in the absence of a mean flow. It may be readily concluded [*Hughes*, 1995, 1996; *Hughes et al.*, 1998; *Smith and Marshall*, 2009] that eastward propagation of eddy features in the ACC region is the result of advection by the eastward mean flow. This is reiterated by a detailed comparison of the zonal phase speed and mean dynamic topography fields: there is a remarkable spatial coincidence between the highest eastward phase speeds (surpassing 0.06 m s^{-1}, see Figure 2d) and the fastest jets (exceeding 0.2 m s^{-1}, see Figure 2a). Note, however, that the difference between the mean flow and eddy phase speeds (or $U_m - c$) is larger in the main jets than in regions of weak mean flow. This observation implies, following (8), that κ is suppressed in the jets, i.e., water parcels are advected rapidly past eddying motions and so the extent to which eddies stir tracers is reduced locally.

[44] The eddy field, though, is comprised of more than a single dominant frequency σ and phase speed c. Unlike the monochromatic version of the stochastic fluctuation-dissipation model used to obtain (8), the eddy field is multi-chromatic and has both barotropic and baroclinic components. Rather than formulating a representation that includes such refinements, *Ferrari and Nikurashin* [2010] conduct a comprehensive test of the scaling law in (8) with altimetric data and find a suppression in κ of up to a factor of 2–3 in the core of the ACC jets. They show that an accurate approximation to (8) is given by

$$\kappa = \frac{\kappa_{Taylor}}{1+4U_m^2 EKE^{-1}}. \quad (10)$$

Combining typical values of U_m and EKE (cf. Figures 2a and 2b) in (10) predicts a reduction in κ of 20%–70% in the ACC core with hardly any impact on the current's

flanks (cf. Figure 2c), in broad agreement with the findings of studies discussed in Section 4.2. We contend, however, that as these studies rely exclusively on relatively coarse [O(100 km)] altimetric observations or eddy-permitting model output, the suppression of κ is likely to be underestimated. Indeed, the *in situ* measurements analyzed in Section 3 suggest that the ACC jets are both narrower and faster than estimated from those coarse data sets, which would result in a larger term in the denominator of (8) or (10) and a predicted stronger suppression of κ.

[45] In order to more rigorously assess the extent to which the weakly nonlinear eddy ideas are consistent with our analysis of the thermohaline fine structure of hydrographic sections, the locations of the transects analyzed in section 3 are overlaid on a map of the inverse stirring suppression factor, defined as the inverse of the denominator in (10), $(1 + 4U_m^2\, EKE^{-1})^{-1}$, and calculated using the mean surface flow of *Maximenko and Niiler* [2005] (Figure 2a) and an altimetric estimate of EKE (Figure 2b). Values near 1 (0) of this factor predict the absence (presence) of stirring suppression. Squares along the sections denote the mean dynamic topography values of the jets at which mixing length suppression is indicated by the hydrography, while circles mark jets where no suppression is observed in the *in situ* measurements. Overall, there is a good correspondence between the theoretical predictions and the *in situ* estimates of suppression, but for two ambiguous cases (the PF in WOCE I6S and WOCE I8S) and two obvious exceptions (the SAF in WOCE SR1b and the northern branch of the SAF in WOCE SR3). Significantly, three of these four ambiguous or exceptional jets were identified as leaky by our analysis of the hydrography. While the lack of mesoscale detail in the map in Figure 2c prevents us from categorizing these three jets as being clearly inconsistent with the weakly nonlinear eddy theory, the hydrographic analysis of those jet regions reveals the presence of strong and narrow mean flows with no mixing length suppression. This pattern is incompatible with the prediction of equations (8) and (10), and will serve to motivate our subsequent discussion of eddy stirring across a narrow and twisted jet in the next subsection.

[46] An alternative, more succinct way of visualizing the same conclusion is illustrated by Figure 11, which displays averages of L_{mix} estimates as a function of the inverse stirring suppression factor for the three leaky jets and for the remainder of the analyzed sections. Whereas the latter group of estimates is quantitatively consistent with the predictions of weakly nonlinear eddy theory, the former set of estimates suggests a local increase in L_{mix} (and κ) for $(1 + 4U_m^2\, EKE^{-1})^{-1} < 0.3$, and thus deviates markedly from those predictions.

4.4. Eddy Stirring Across a Narrow, Twisted Jet

4.4.1. Concept

[47] The theory underpinning expressions (7)–(9) relies on two major assumptions that are not always satisfied in the ACC: (1) that a separation between the length scales of the jet and the eddies exists; and (2) that the mean flow is zonal or, more generally, a parallel shear flow with velocity gradients in the vertical and only *one* horizontal direction. Studies of mixing across a narrow parallel Bickley jet [*Rypina et al.*, 2007] show that, for parallel shear flows, mixing suppression continues to hold even in the absence of scale separation, such that the first assumption above is not critical. In contrast, there are firm indications of the theory's predictions being shaped decisively by the second assumption.

[48] Passive scalar dynamics is greatly enriched when a jet is twisted (non-parallel). Key illustrations of how such richness comes about may be found in past studies of the roles of the (isentropic) rate of strain [*Okubo*, 1970; *Weiss*, 1991] and Lagrangian acceleration [*Hua and Klein*, 1998] in shaping the stirring properties of a 2-d turbulent fluid. A finding of those investigations is that non-parallel flows host an exponential separation of particle pairs with time, rather than the asymptotically much slower linear separation with time that is characteristic of parallel flows. The rapid increase in particle separation is associated with twisting and folding of tracer filaments and thereby promotes a local intensification of cross-stream tracer fluxes. This translates into an enhancement of the eddy diffusivity κ relating the magnitude of the tracer flux to the background tracer gradient in the region of the straining mean flow. The behavior of linear waves in non-parallel, horizontally non-divergent background flows is, in the limit of an extreme scale separation between the waves and the background, analogous to that of passive scalars [*Bühler and McIntyre*, 2005; *Polzin*, 2008]. While the complicated aspects of non-parallel flows render the problem analytically intractable, a recent highly idealized numerical study by *Thompson* [2010] shows that cross-jet mixing indeed ceases to be suppressed if the background PV gradient has small-scale non-parallel structure. Thompson generated such a background PV gradient with topographic hills, but we may expect to see a similar behavior of eddy stirring regardless of the specific mechanism that maintains sharp and non-parallel PV gradients. Thus, following this argument, we anticipate that a breakdown of mixing suppression may occur in narrow, non-parallel jets.

[49] Although no generalized theory yet exists to predict the detailed distribution of κ in non-parallel flows, the Okubo-Weiss parameter (D) has been shown to be a useful indicator of regions where particle separation increases exponentially and jets are likely to become leaky [e.g., *Haller and Yuan*, 2000]. The Okubo-Weiss parameter is defined as

$$D = \frac{S_n^2 + S_s^2 - \Gamma^2}{4}, \tag{11}$$

where $S_n = \partial u/\partial x - \partial v/\partial y$ is the normal component of the rate of strain, $S_s = \partial v/\partial x + \partial u/\partial y$ is the shear component of the rate of strain, and $\Gamma = \partial v/\partial x - \partial u/\partial y$ is the vertical component of the relative vorticity [*Okubo*, 1970; *Weiss*, 1991]. In the limit of small particle pair separation in a horizontally nondivergent, 2-d turbulent velocity field, $|D|^{-1/2}$ is a characteristic time scale of exponential particle pair separation in straining elements of the flow (for which $D > 0$), whereas it is a characteristic time scale of the variation in the relative orientation of particle pairs in vortical elements of the flow (for which $D < 0$). Parallel flows fall into a special category of $D \equiv 0$ and linear (asymptotically slow) particle pair separation.

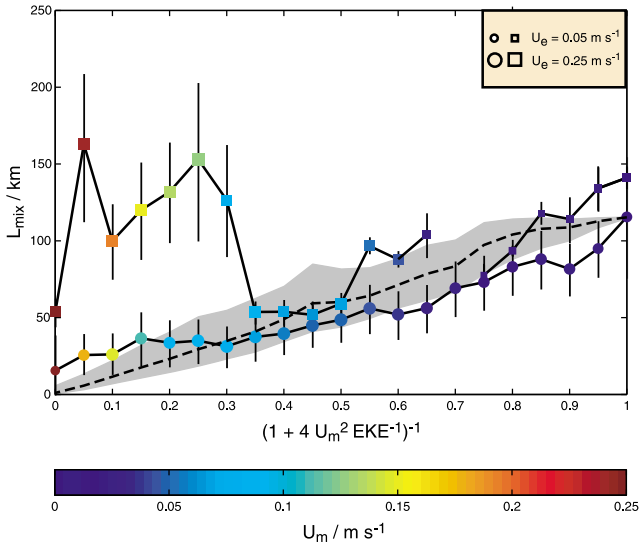

Figure 11. L_{mix} estimates (colored symbols, shaded by the average U_m) from the five sections analyzed here, averaged in bins of inverse stirring suppression factor $(1 + 4U_m^2 EKE^{-1})^{-1}$. Squares show averages of L_{mix} estimates from the three leaky jet regions identified in section 3 (the SAF in WOCE SR1b, the PF south of Africa and the SAF's northern branch south of Tasmania). Circles show averages of L_{mix} estimates from the remainder of the sections. L_{mix} values greater than 700 km (mostly below 2000 m) or from the uppermost 100 m of the water column are disregarded in the averaging. The size of each symbol denotes the average value of U_e in each bin (see inset), and the vertical lines the standard deviation of individual L_{mix} estimates in each bin. The dashed line shows the structure of L_{mix} predicted by the inverse stirring suppression factor in (10), using the observed L_{mix} value at $(1 + 4U_m^2 EKE^{-1})^{-1} = 1$, the relation $EKE = U_e^2$, and the average U_m and U_e values in each bin. The grey shading indicates the range of predicted L_{mix} values associated with one standard deviation of the individual estimates of U_m and U_e in each bin.

4.4.2. Assessment

[50] In order to assess whether the absence of eddy stirring suppression observed in a small subset of the jets in the hydrographic sections may conceivably be interpreted in terms of the preceding ideas, we calculate the Okubo-Weiss parameter of the mean surface flow from *Maximenko and Niiler*'s [2005] mean dynamic topography. Given the small number of jets in which stirring suppression is absent, this assessment is necessarily exploratory. The result of the calculation is shown in Figure 2e. We find that the mean streamlines associated with the three exceptional, high κ upper-ocean jets (the SAF in WOCE SR1b, the PF in WOCE I6S, and the SAF's northern branch in WOCE SR3) meander through alternating patches of large strain ($D \gg 10^{-13}$ s^{-2}) and vorticity ($D \ll -10^{-13}$ s^{-2}) closely upstream of the sections at which they are sampled, whereas conventional stirring barrier jets are widely characterized by small values of D indicative of parallel flow (with one obvious exception, the SAF in WOCE S1, which will be discussed in the following section). This suggests that the breakdown of stirring suppression in certain segments of the ACC jets may be plausibly attributed to the occurrence of non-parallel conditions in those segments. Following from this, we hypothesize that ACC jets become leaky in regions of large mean flow strain (such as when a jet is narrow and twisted), while they act as barriers to eddy stirring elsewhere.

[51] If our hypothesis regarding the breakdown of suppression in non-parallel flows is valid, some insight into the dynamics controlling the degree of leakiness of ACC jets may be obtained by close examination of the spatial distribution of the straining and vortical elements in the time mean velocity field, as revealed by the Okubo-Weiss parameter (Figure 2e). Two features of this distribution are most readily apparent. First, straining and vortical elements of the flow commonly occur in sets of alternating patches associated with meanders in the mean flow that have characteristic wavelengths of 300–500 km. Second, the occurrence of these patches is neither ubiquitous nor seemingly random, but it is focussed on relatively confined regions of strong mean flow in the vicinity of complex topography. See, in particular, the isolated areas of positive and negative D over the Southwest Indian Ridge near WOCE I6S, the trains of straining and vortical patches around the northern edges of the Del Ca no Rise and the Kerguelen Plateau between 40°E and 80°E, the region around the northern flank of the Southeast Indian Ridge between 95°E and 120°E, the region of Macquarie Ridge and Campbell Plateau, south of Tasmania and New Zealand, the Udintsev and Eltanin Fracture Zones, around 140°W, and finally the northern Scotia Sea and neighboring basins to the north.

[52] The character of the meander trains was investigated by *Hughes* [2005] in the course of a study of the ACC's near-surface vorticity balance. He found the meanders to have properties akin to those of short (compared to $2\pi L_R$, where $L_R \approx 2000$ km is the barotropic Rossby radius of deformation) westward-propagating barotropic Rossby waves held stationary by the mean flow, as illustrated most clearly by the meanders' nonlinear vorticity balance (not shown here). The clustering of the meanders around areas of complex bathymetry indicates that they are 'lee waves', generated by the interaction of the ACC flow with topographic obstacles in the manner characterized by e.g., *Tansley and Marshall* [2001] and *Rhines* [2007]. The topographic localization of eddy stirring suggested by our analysis is reminiscent of the findings of *MacCready and Rhines* [2001] in numerical simulations of an idealized channel flow over topography, although the extent to which the processes discussed here operate in their model is unclear.

[53] To conclude, we must caution that our estimate of L_{mix}, based on equation (3), formally assumes a separation in scale between the eddy mixing length and the large-scale θ gradient. The above analysis suggests that the three regions in which suppression of L_{mix} was not found at jets are characterized by the existence of sharp meanders in the mean flow, which may violate the scale separation assumption. Hence, careful analysis of numerical simulations is likely required to confirm the breakdown of eddy stirring suppression in non-parallel jets, and to settle the dynamics at work.

4.5. Near-Boundary Turbulent Suppression

4.5.1. Concept

[54] A final theoretical ingredient is required to complete our interpretation of the observed patterns of eddy stirring in the hydrographic transects. This is commonly referred to as near-boundary turbulent suppression or 'law of the wall' [e.g., *Tennekes and Lumley*, 1972] and states that in the presence of a solid boundary, the physical scales of eddies are limited by the distance to the boundary. It is thus reasonable to expect that the eddy mixing length L_{mix}, as a root-mean-square measure of cross-stream particle displacements, and therefore κ are to be similarly constrained.

4.5.2. Assessment

[55] In section 4.4.2, we found that one of the jets in the hydrographic sections (the SAF in WOCE S1) meanders through alternating patches of large strain and vorticity closely upstream of the S1 transect (Figure 2e), yet the hydrographic analysis revels that it is not leaky. This is at odds with the discussion of eddy stirring across non-parallel jets in section 4.4. We contend that the absence of a strain-related breakdown of mixing suppression in this jet can be readily explained by invoking the law of the wall. As shown by *Garabato et al.* [2003] and hinted at by Figure 4e, the SAF jet in western Drake Passage overlies a very steep segment of the South American continental slope, suggesting that the suppression of eddy stirring across the jet is simply the result of a reduction of L_{mix} in the proximity of a boundary. The downstream evolution of the jet's mixing characteristics appears to support this explanation. By the time it crosses the WOCE SR1b section in eastern Drake Passage, the SAF jet has moved off the continental slope (Figure 5e) and, with increasing distance from the boundary, becomes leaky (Figure 5d).

5. Conclusions

[56] The character of eddy stirring in the Southern Ocean has been investigated by analyzing a collection of hydrographic transects and spatially coincident altimetric measurements within a mixing length theoretical framework. The outcomes of this analysis provide significant insight into the long-standing debate concerning the distribution of eddy stirring across the ACC and the nature of its controlling processes.

[57] We have shown that, typically, the isentropic eddy diffusivity κ is reduced by an order of magnitude in the upper O(1 km) of the ACC frontal jets relative to their surroundings. The spatial structure of κ primarily results from variability in the eddy mixing length: L_{mix} is not simply proportional to the physical scale of eddies, as it is often assumed in the oceanographic literature [e.g., *Holloway*, 1986; *Visbeck et al.*, 1997; *Salmon*, 1998], rather it is modified by eddy-mean flow interactions. This characteristic behavior of mixing is reproduced and illuminated by a quasi-geostrophic theory of eddy stirring across a broad barotropic jet founded on the work of *Ferrari and Nikurashin* [2010]. The theory indicates that the observed widespread reduction of L_{mix} and κ in the upper layers of frontal jets is the kinematic consequence of eddy propagation relative to the mean flow within jet cores. As shown by other investigators in the past [e.g., *Hughes et al.*, 1998], eddying motions in the ACC propagate eastward considerably more slowly than the surface mean flow does. The lack of mixing suppression outside and in the deep [O(>1 km)] layers of jet centers may thus be attributed to the tendency of the eddy propagation relative to the mean flow to become small there.

[58] While the inferred spatial distribution of κ across the ACC shares several basic features with patterns highlighted by the model-based studies of *Smith and Marshall* [2009] and *Abernathy et al.* [2009], amongst others, our interpretation of those features differs. Based on both observational and theoretical leads, we suggest that the prevalent control on the κ distribution is the *suppression* of eddy stirring at the center of the jets, rather than the *enhancement* of κ above background values at Rossby wave critical layers girdling the jets. Most fundamentally, we contend that the characteristic thermohaline structure of the ACC, consisting of multiple upper-ocean thermohaline fronts separating and underlaid by regions of homogenized properties, is largely a result of *suppression* of eddy stirring by eddy-mean flow interactions outlined above.

[59] As widely valid as this characterization of eddy stirring is likely to be, our analysis reveals that it is not universally applicable across the Southern Ocean. Pronounced deviations from the prevalent mixing regime are encountered in a few special sites. There, mixing suppression is observed to break down at the core of upper-ocean jets, allowing intense cross-stream exchange of thermohaline properties to ensue. The key condition associated with the emergence of such leaky jet segments is tentatively identified as the occurrence of non-parallel structure in the mean flow on length scales comparable to those of the eddies. In the light of the limited available evidence, the Okubo-Weiss parameter of the mean flow has some skill as a qualitative indicator of the satisfaction of this condition. While no generalized theory of mixing in a non-parallel mean flow yet exists, a number of past studies have shown that passive scalar and linear wave dynamics is greatly enriched in straining flows, as a result of their hosting a much faster along-stream particle pair separation and sharpening of cross-stream tracer gradients. In the case of the ACC, the mean flow strain that likely underpins the breakdown of mixing suppression occurs within sharp stationary meanders of 300–500 km wavelength. These can be characterized as short westward-propagating barotropic Rossby waves that are generated by the interaction of the ACC with topography and held stationary by the mean flow. Such association between stationary meanders and prominent bathymetric features provides a plausible explanation for the relatively rare occurrence of leaky jet segments in the ACC, and suggests that complex eddy- mean flow interaction dynamics are at play in regions of strong topographic steering and form drag.

[60] We conjecture that these localized disruptions to the regular 'mixing barrier' behavior of upper-ocean jets may underlie the abrupt along-stream changes in water mass properties and frontal structure that have been reported to occur as the ACC negotiates major topographic obstacles [*Sallée et al.*, 2010; *Thompson et al.*, 2011]. Recalling that the rate of eddy-induced meridional circulation is proportional to the eddy PV flux (see discussion by, e.g., *Olbers et al.* [2004]), our observation of leaky jet segments hosting both high values of κ and large isopycnal PV gradients

suggests that those sites contribute disproportionally to the eddy-induced overturning across the ACC and the associated maintenance of the Southern Ocean stratification. Extant estimates of the residual overturning and associated stratification assume that κ is constant or enhanced at jets [e.g., *Olbers and Visbeck*, 2005; *Marshall and Radko*, 2006]. Our results show that these assumptions are inconsistent with the eddy-mean flow interactions that so profoundly shape the thermohaline structure of the Southern Ocean.

Appendix A: Sensitivity Analysis of the Calculation of the Eddy Mixing Length Scale L_{mix}

[61] Our calculation of the eddy mixing length L_{mix} involves several somewhat subjective parameter choices, and assumes that each of the hydrographic section data sets has sufficient lateral resolution to resolve the spatial patterns (in particular, transitions from jet to inter-jet regions) in L_{mix}. In this Appendix, we describe the impact that the various parameters have in our calculation results, and define the minimum spatial density of hydrographic station sampling that is required to resolve the essential features of the L_{mix} distribution.

A1. Influence of Parameter Choices in the L_{mix} Calculation Results

[62] Our calculation of L_{mix} involves the choice of four parameters. First, the isobaric levels for the definition of a dynamic height coordinate are selected. In practice, this choice has a barely detectable impact (below the 1% level) in the resulting L_{mix}, for the equivalent barotropicity of the ACC implies that all dynamic height variables are essentially linearly dependent on one another.

[63] Second, a relationship between the dynamic height coordinate of choice and along-section distance is determined by fitting a cubic spline to the measured data points, in order to define a cross-stream pseudo-distance Y. The imposed smoothness of the spline can influence the width of frontal jet regions, in which dynamic height changes rapidly (and occasionally non-monotonically) with distance. Typically, the range of reasonable choices of spline smoothing parameter lead to changes in jet widths of up to ~20 km (i.e., around 20% of a characteristic jet width of 100 km), but have little impact (generally below the 10% level) in the magnitude of L_{mix}.

[64] Third, the background potential temperature θ_m is defined by fitting a cubic spline to the measured (θ, Y) data pairs. The calculated L_{mix} changes little (generally by less than 10%) within the range of reasonable choices of spline smoothing parameter. The only exception is found in several spatially confined areas where isoneutral surfaces outcrop near the ACC's Southern Boundary. There, the sharp isoneutral potential temperature gradient characterizing the base of the winter mixed layer is not well captured by some choices of spline smoothing parameter. This localized issue has little bearing on the estimated large-scale distribution of L_{mix}.

[65] Fourth, the calculation of L_{mix} involves the specification of a pseudo-distance interval ΔY. This parameter defines the half-width of a running window within which θ_{rms} is computed as the one standard deviation of the departures of measured potential temperature from the local θ_m. Experimentation with different values of ΔY shows that the parameter must be large enough for the calculation window to encompass at least 5–10 measurements, if the calculation is to converge. In practice, this translates into ΔY values of 30–150 km, depending on the spatial resolution of the sampling and the width of the ACC at each section location. For smaller values of ΔY, the calculated L_{mix} distribution is overly noisy, to the point that identification of the basic patterns is compromised. Given this constraint, the magnitude of L_{mix} exhibits relatively weak sensitivity to the value of ΔY, varying by O(10%) over the stated ΔY range. If ΔY is taken to be O(300 km) or larger, the spatial patterns in L_{mix}, which have a characteristic lateral scale comparable to 100 km, begin to be blurred beyond recognition. In the end, the requirement of having a certain number of data points (5–10) within this characteristic distance (100 km) sets the baseline sampling density that a section must have in order to yield useful information on L_{mix}. Next, we show that such baseline is roughly equivalent to two repeats of a hydrographic section with WOCE-standard station spacing.

A2. Spatial Density of Hydrographic Station Sampling Required for the L_{mix} Calculation

[66] We now use the SR1b data set at eastern Drake Passage, which consists of over 300 stations collected during 10 section repeats, to show that the basic patterns of the L_{mix} distribution can be recovered from any pair of transects, typically encompassing 60 stations. This point is illustrated by Figure A1, which displays the lateral distribution of L_{mix} calculated from the ten section repeats alongside the one standard deviation envelope of L_{mix} estimates obtained from all combinations of pairs of SR1b transects, for four distinct neutral surfaces. It can be seen that, despite its substantial width, the envelope of section-pair estimates reproduces the main features of the L_{mix} distribution calculated from the complete SR1b data set, i.e., the minima in L_{mix} north of the SAF for the two lightest density surfaces, at the PF for the three lightest levels, and at the SBdy for γ^n = 28.0 kg m^{-3}; and the higher L_{mix} values at the SAF, south of the PF for the three lightest surfaces, and across much of the ACC at the densest level.

[67] Based on this evidence, we regard the spatial density of sampling associated with the number of stations in two SR1b transects (about 5–10 stations per 100 km) as a reasonable baseline value required for the L_{mix} calculation to capture the basic patterns in the mixing length distribution. Whereas one-time WOCE sections typically fall short of this baseline, the specification is met by the five section data sets considered in this study.

Appendix B: Interpretation of Thermohaline Variability on Isopycnal Surfaces

[68] Our conceptual framework for interpreting isopycnal thermohaline variability in the Southern Ocean is grounded in the triple decomposition of *Joyce* [1977] and *Joyce et al.* [1978], which invokes mean ($\bar{\phi}$), intermediate production ($\tilde{\phi}$) and dissipation (ϕ') scales for any scalar variable ϕ. In regions of significant isopycnal thermohaline gradients, the

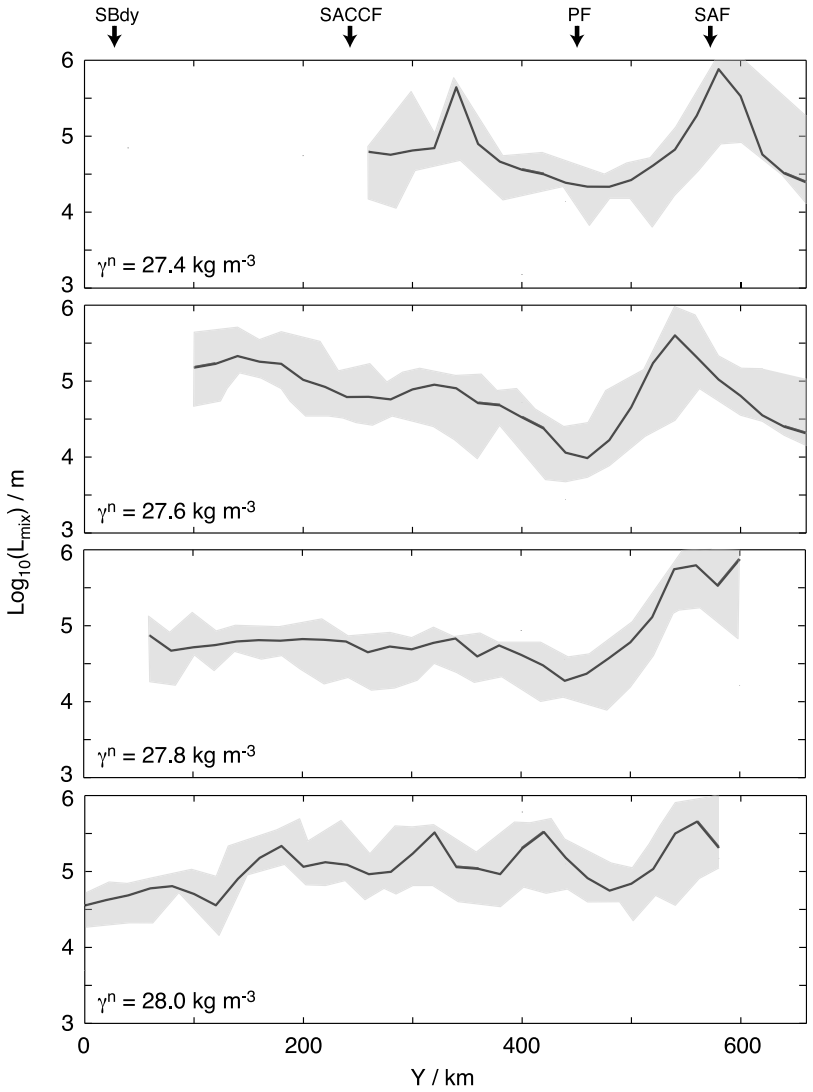

Figure A1. Distribution of $\log_{10}$ (L_{mix}) as a function of Y for four neutral density surfaces (γ^n values indicated in the lower left hand corner of each panel) along the WOCE SR1b section. The black line shows the L_{mix} distribution calculated from ten repeats of the section. The gray-shaded area indicates the one standard deviation envelope of the L_{mix} distributions calculated from all possible pairs of WOCE SR1b section repeats, centered around the mean of all such distributions. The positions of hydrographic fronts are indicated at the top of each set of panels and labeled as in Figures 1 and 2.

mean potential temperature *variance* budget reduces [*Joyce*, 1977] to a dominant balance between isopycnal production

$$\overline{\tilde{v}\tilde{\theta}}\frac{\partial\overline{\theta}}{\partial y} \cong -\kappa\frac{\partial\overline{\theta}^2}{\partial y}$$

and dissipation

$$\overline{w'\theta'}\frac{\partial\overline{\theta}}{\partial z} \cong -K_\rho\overline{\left[\frac{\partial\tilde{\theta}}{\partial z}\right]^2},$$

where v and w respectively denote cross-frontal isopycnal and diapycnal velocities and K_ρ is a small-scale diapycnal diffusivity. It follows that

$$\kappa \cong K_\rho\overline{\left[\frac{\partial\tilde{\theta}}{\partial z}\right]^2} \Big/ \left[\frac{\partial\overline{\theta}}{\partial y}\right]^2.$$

This balance holds irrespectively of whether thermohaline fine structure is considered to result from mesoscale eddy stirring and to be completely density-compensating (i.e., a passive tracer), or whether it is regarded as being created in conjunction with small-scale diapycnal processes as in the case of double-diffusively driven intrusions (i.e., an active tracer). While one can argue about what K_ρ value is most appropriate and whether $\overline{\left[\tilde{\theta}_z\right]^2}$ is adequately resolved by a given set of observations, that balance leads to $\kappa \sim O(10)$ $m^2\ s^{-1}$ in the Polar Front if a characteristic observed value of the ratio $\overline{\left[\tilde{\theta}_z\right]^2}/[\overline{\theta}_y]^2$ ($\sim O(10^5)$ [see *Joyce et al.*, 1978]) and an upper-limit value of $K_\rho = 1 \times 10^{-4}$ $m^2\ s^{-1}$ are adopted. A smaller value of K_ρ yields an even weaker rate of isopycnal stirring. Thus, regardless of whether one considers isopycnal thermohaline variability to represent a passive or dynami-

cally active process, the rate of isopycnal stirring is small at the core of ACC frontal jets, consistent with our findings.

[69] The interpretation of isopycnal thermohaline variability as being produced by double diffusive processes put forward by *Joyce et al.* [1978] is motivated by the small vertical scales and characteristic aspect ratios of interleaving features. Specifically, their interpretation builds on the following characteristics of thermohaline filaments: (1) vertical scales of 50–100 m; (2) a typical slope of $2–4 \times 10^{-2}$, much steeper than isopycnals; and (3) an increase in the density of the filaments as they cross the jets, though this last characterization requires caveats [*Toole*, 1981]. We argue that all these properties are consistent with the eddy stirring scenario put forward here. *Smith and Ferrari* [2009] show that along-isopycnal eddy advection generates filaments that are thin in the horizontal (through eddy strain) and in the vertical (through eddy shear). The thinning of filaments by mesoscale eddies is eventually arrested at vertical scales of 10–100 m (consistent with *Joyce et al.* [1978]) by a vertical diffusivity of 1×10^{-5} m^2 s^{-1} acting equally upon temperature and salinity profiles. *Smith and Ferrari* [2009] further demonstrate that the resulting filaments have an aspect ratio proportional to f/N. With values of $f = 1.2 \times 10^{-4}$ s^{-1} and $N = 3 \times 10^{-3}$ s^{-1} as observed by *Joyce et al.* [1978], this aspect ratio $f/N \approx 4 \times 10^{-2}$ is consistent with the observations reported in that study. Finally, the filaments generated by eddy stirring have density ratios close to 1 and are susceptible to double-diffusive instabilities that act to increase their density. Hence filaments *could* slope across isopycnals in response to double-diffusive fluxes. We note, however, that double diffusion is not the process generating the filaments, but instead is a consequence of eddy stirring and results in a slight modification of filament densities. We thus conclude that the thermohaline filaments observed across the ACC are likely the result of isopycnal eddy stirring: there is no shortage of eddy activity in the Southern Ocean. Other interpretations would be warranted only if the observed filaments had characteristics inconsistent with the eddy stirring scenario, and this is presently not the case.

[70] **Acknowledgments.** This study was conducted during A.C.N. G.'s stay at MIT, which was supported jointly by MIT and the U.K. Natural Environment Research Council (NERC) through a NERC Advanced Research Fellowship (NE/C517633/1). R.F. acknowledges the support of NSFaward OCE-0825376. K.P.'s participation in this work was supported by WHOI bridge support funds. We are grateful to David Marshall, Alan Plumb, Peter Rhines, Bernadette Sloyan, Andy Thompson and Jan Zika for helpful discussions; Rob Scott for advice with the analysis of altimetric observations; and Chris Hughes for providing the altimetric estimate of zonal wave speed reproduced in Figure 2d.

References

Abernathy, R., J. Marshall, M. Mazloff, and E. Shuckburgh (2009), Studies of enhanced isopycnal mixing at deep critical levels in the Southern Ocean, *J. Phys. Oceanogr.*, *40*, 170–184.

Armi, L., and H. Stommel (1983), Four views of a portion of the North Atlantic Subtropical Gyre, *J. Phys. Oceanogr.*, *13*, 828–857.

Bower, A. S., and M. S. Lozier (1994), A closer look at particle exchange in the Gulf Stream, *J. Phys. Oceanogr.*, *26*, 1399–1418.

Bower, A. S., and H. T. Rossby (1989), Evidence of cross-frontal exchange processes in the Gulf Stream based on isopycnal RAFOS float data, *J. Phys. Oceanogr.*, *19*, 1177–1190.

Bower, A. S., H. T. Rossby, and J. L. Lillibridge (1985), The Gulf Stream —barrier or blender?, *J. Phys. Oceanogr.*, *15*, 24–32.

Bryden, H. L., and S. A. Cunningham (2003), How wind forcing and the air-sea heat exchange determine meridional temperature gradient and stratification for the Antarctic Circumpolar Current, *J. Geophys. Res.*, *108*(C8), 3275, doi:10.1029/2001JC001296.

Bühler, O., and M. E. McIntyre (2005), Wave capture and wave-vortex duality, *J. Fluid Mech.*, *534*, 67–95.

Cerovečki, I., R. A. Plumb, and W. Heres (2009), Eddy transport and mixing in a wind- and buoyancy-driven jet on the sphere, *J. Phys. Oceanogr.*, *39*, 1133–1149.

Chelton, D. B., M. G. Schlax, R. M. Samelson, and R. A. de Szoeke (2007), Global observations of large oceanic eddieS, *Geophys. Res. Lett.*, *34*, L15606, doi:10.1029/2007GL030812.

Dritschel, D. G., and M. E. McIntyre (2008), Multiple jets as PV staircases: The Phillips effect and the resilience of eddy-transport barriers, *J. Atmos. Sci.*, *65*, 855–874.

Farrell, B. F., and P. J. Ioannou (1993), Stochastic forcing of the linearized Navier-Stokes equations, *Phys. Fluids*, *A5*, 2600–2609.

Ferrari, R., and M. Nikurashin (2010), Suppression of eddy mixing across jets in the Southern Ocean, *J. Phys. Oceanogr.*, *40*, 1501–1519.

Ferrari, R., and K. L. Polzin (2005), Finescale structure of the T-S relation in the eastern North Atlantic, *J. Phys. Oceanogr.*, *35*, 1437–1454.

Ferreira, D., J. Marshall, and P. Heimbach (2005), Estimating eddy stresses by fitting dynamics to observations using a residual-mean ocean circulation model and its adjoint, *J. Phys. Oceanogr.*, *35*, 1891–1910.

Flierl, G. R., and D. J. McGillicuddy (2002), Mesoscale and submesoscale physical-biological interactions, in *Biological-Physical Interactions in the Sea, The Sea*, vol. 12, edited by J. J. McCarthy, B. J. Rothschild, and A. R. Robinson, pp. 113–185, Wiley, Hoboken, N. J.

Garabato, A. C. N., D. P. Stevens, and K. J. Heywood (2003), Water mass conversion, fluxes and mixing in the scotia sea diagnosed by an inverse model, *J. Phys. Oceanogr.*, *33*, 2565–2587.

Garabato, A. C. N., K. L. Polzin, B. A. King, K. J. Heywood, and M. Visbeck (2004), Widespread intense turbulent mixing in the Southern Ocean, *Science*, *303*, 210–213.

Green, J. S. A. (1970), Transfer properties of the large-scale eddies and the general circulation of the atmosphere, *Q. J. R. MeteorOL. Soc.*, *96*, 157–185.

Haller, G., and G. Yuan (2000), Lagrangian coherent structures and mixing in two-dimensional turbulence, *Phys. D*, *147*, 352–370.

Haynes, P. H., and E. Shuckburgh (2000a), Effective diffusivity as a diagnostic of atmospheric transport: 1. Stratosphere, *J. Geophys. Res.*, *105*, 22,777–22,794.

Haynes, P. H., and E. Shuckburgh (2000b), Effective diffusivity as a diagnostic of atmospheric transport: 2. Troposphere and lower stratosphere, *J. Geophys. Res.*, *105*, 22,795–22,810.

Held, I., and V. D. Larichev (1996), A scaling theory for horizontally homogeneous, baroclinically unstable flow on a beta-plane, *J. Atmos. Sci.*, *53*, 946–952.

Holloway, G. (1986), Estimation of oceanic eddy transports from satellite altimetry, *Nature*, *323*, 243–244.

Holloway, G., and S. S. Kristmannsson (1984), Stirring and transport of tracer fields by geostrophic turbulence, *J. Fluid Mech.*, *141*, 27–50.

Hua, B. L., and P. Klein (1998), An exact criterion for the stirring properties of nearly two-dimensional turbulence, *Phys. D*, *113*, 98–110.

Hughes, C. W. (1995), Rossby waves in the southern ocean: A comparison of TOPEX/POSEIDON altimetry with model predictions, *J. Geophys. Res.*, *100*, 15,933–15,950.

Hughes, C. W. (1996), The Antarctic Circumpolar Current as a waveguide for Rossby waves, *J. Phys. Oceanogr.*, *26*, 1375–1387.

Hughes, C. W. (2005), Nonlinear vorticity balance of the Antarctic Circumpolar Current, *J. Geophys. Res.*, *110*, C11008, doi:10.1029/2004JC002753.

Hughes, C. W., M. S. Jones, and S. Carnochan (1998), Use of transient features to identify eastward currents in the southern ocean, *J. Geophys. Res.*, *103*, 2929–2944.

Jackett, D. R., and T. J. McDougall (1997), A neutral density variable for the world's oceans, *J. Phys. Oceanogr.*, *27*, 237–263.

Joyce, T. M. (1977), A note on the lateral mixing of water masses, *J. Phys. Oceanogr.*, *7*, 626–629.

Joyce, T. M., W. Zenk, and J. M. Toole (1978), The anatomy of the Antarctic Polar Front in the Drake Passage, *J. Geophys. Res.*, *83*, 6093–6114.

Karsten, R. H., and J. Marshall (2002), Constructing the residual circulation of the ACC from observations, *J. Phys. Oceanogr.*, *32*, 3315–3327.

Karsten, R. H., H. Jones, and J. Marshall (2002), The role of eddy transfer in setting the stratification and transport of a circumpolar current, *J. Phys. Oceanogr.*, *32*, 39–54.

Keffer, T., and G. Holloway (1988), Estimating southern ocean eddy flux of heat and salt from satellite altimetry, *Nature*, *332*, 624–626.

Killworth, P. D. (1997), On the parameterization of eddy transfer. Part 1: Theory, *J. Mar. Res.*, *55*, 1171–1197.

Landahl, M. T. (1975), Wave breakdown and turbulence, *SIAM J. Appl. Math.*, *28*, 735–756.
Lozier, M. S., L. J. P. A. M. Rogerson, and P. D. Miller (1997), Exchange geometry revealed by float trajectories in the Gulf Stream, *J. Phys. Oceanogr.*, *27*, 2327–2341.
MacCready, P., and P. B. Rhines (2001), Meridional transport across a zonal channel: Topographic localization, *J. Phys. Oceanogr.*, *31*, 1427–1439.
Marshall, D. P. (1997), Subduction of water masses in an eddying ocean, *J. Mar. Res.*, *55*, 201–222.
Marshall, J., and T. Radko (2003), Residual mean solutions for the Antarctic Circumpolar Current and its associated overturning circulation, *J. Phys. Oceanogr.*, *33*, 2341–2354.
Marshall, J., and T. Radko (2006), A model of the upper branch of the meridional overturning circulation of the Southern Ocean, *Prog. Oceanogr.*, *70*, 331–345.
Marshall, J., E. Shuckburgh, H. Jones, and C. Hill (2006), Estimates and implications of surface eddy diffusivity in the Southern Ocean derived from tracer transport, *J. Phys. Oceanogr.*, *36*, 1806–1821.
Maximenko, N. A., and P. P. Niiler (2005), Hybrid decade-mean global sea level with mesoscale resolution, in *Recent Advances in Marine Science and Technology, 2004*, edited by N. Saxena, pp. 55–59, PACON Int., Honolulu.
Nakamura, N. (1996), Two-dimensional mixing, edge formation, and permeability diagnosed in area coordinates, *J. Atmos. Sci.*, *53*, 1524–1537.
Okubo, A. (1970), Horizontal dispersion of floatable particles in the vicinity of velocity singularities such as convergences, *Deep Sea Res.*, *17*, 445–454.
Olbers, D., and M. Visbeck (2005), A model of the zonally averaged stratification and overturning in the Southern Ocean, *J. Phys. Oceanogr.*, *35*, 1190–1205.
Olbers, D., D. Borowski, C. Völker, and J.-O. Wolff (2004), The dynamical balance, transport and circulation of the Antarctic Circumpolar Current, *Ant. Sci.*, *16*, 439–470.
Pierrehumbert, R. T. (1991), Chaotic mixing of tracers and vorticity by modulated travelling Rossby waves, *Geophys. Astrophys. Fluid Dyn.*, *58*, 285–319, doi:10.1080/03091929108227343.
Polzin, K. L. (2008), Mesoscle eddy–internal wave coupling. PartI. Symmetry, wave capture and results from the Mid-Ocean Dynamics Experiment, *J. Phys. Oceanogr.*, *38*, 2556–2574.
Prandtl, L. (1925), Bericht ueber untersuchungen zur ausgebildeten turbulenz, *Z. Angew. Math. Mech.*, *5*, 136–139.
Pratt, L. J., M. S. Lozier, and N. Beliakova (1995), Parcel trajectories in quasigeostrophic jets: Neutral modes, *J. Phys. Oceanogr.*, *25*, 1451–1466.
Randel, W. J., and I. M. Held (1991), Phase speed spectra of transient eddy fluxes and critical layer absorption, *J. Atmos. Sci.*, *48*, 688–697.
Rhines, P. B. (2007), Jets and orography: Idealized experiments with tip jets and lighthill blocking, *J. Atmos. Sci.*, *64*, 3627–3639.
Rhines, P. B., and W. R. Young (1982), A theory of the wind driven circulation. Part I. Mid-ocean gyres, *J. Mar. Res.*, *40*, suppl., 559–596.
Rintoul, S. R., C. W. Hughes, and D. Olbers (2001), The Antarctic Circumpolar Current system, in *Ocean Circulation and Climate*, edited by G. Siedler, J. Church, and J. Gould, pp. 271–302, Academic, New York.
Rogerson, A. M., P. D. Miller, L. J. Pratt, and C. K. R. T. Jones (1999), Lagrangian motion and fluid exchange in a barotropic meandering jet, *J. Phys. Oceanogr.*, *29*, 2635–2655.
Rypina, I. I., M. G. Brown, F. J. Beron-Vera, c. H. Ko, M. J. Olascoaga, and I. A. Udovydchenkov (2007), On the Lagrangian dynamics of atmospheric zonal jets and the permeability of the stratospheric polar vortex, *J. Atmos. Sci.*, *64*, 3595–3610.
Sallée, J.-B., K. Speer, R. Morrow, and R. Lumpkin (2008), An estimate of Lagrangian eddy statistics and diffusion in the mixed layer of the Southern Ocean, *J. Mar. Res.*, *66*, 441–463.
Sallée, J. B., K. Speer, S. R. Rintoul, and S. Wijffels (2010), Southern Ocean thermocline ventilation, *J. Phys. Oceanogr.*, *40*, 509–529.
Salmon, R. (1998), *Lectures on Geophysical Fluid Dynamics*, Oxford Univ. Press, New York.
Schäfer, H., and W. Krauss (1995), Eddy statistics in the south atlantic as derived from drifters drogued at 100 m, *J. Mar. Res.*, *53*, 403–431.
Scott, R. B., and F. Wang (2005), Direct evidence of an oceanic inverse kinetic energy cascade from satellite altimetry, *J. Phys. Oceanogr.*, *35*, 1650–1666.
Smith, K. S. (2005), Tracer transport along and across coherent jets in two-dimensional turbulent flow, *J. Fluid Mech.*, *544*, 133–142.
Smith, K. S., and R. Ferrari (2009), The production and dissipation of compensated thermohaline variance by mesoscale stirring, *J. Phys. Oceanogr.*, *39*, 2477–2501.
Smith, K. S., and J. Marshall (2009), Evidence for enhanced eddy mixing at middepth in the Southern Ocean, *J. Phys. Oceanogr.*, *39*, 50–69.
Speer, K., S. R. Rintoul, and B. Sloyan (2000), The diabatic Deacon cell, *J. Phys. Oceanogr.*, *30*, 3212–3222.
Stammer, D. (1998), On eddy characteristics, eddy transports, and mean flow properties, *J. Phys. Oceanogr.*, *28*, 727–739.
Stone, P. (1972), A simplified radiative-dynamical model for the static stability of the rotating atmosphere, *J. Atmos. Sci.*, *29*, 405–418.
Sun, C., and D. R. Watts (2001), A circumpolar gravest empirical mode for the Southern Ocean hydrography, *J. Geophys. Res.*, *106*, 2833–2855.
Tansley, C. E., and D. P. Marshall (2001), Flow past a cylinder on a β-plane with application to Gulf Stream separation and the Antarctic Circumpolar Current, *J. Phys. Oceanogr.*, *31*, 3274–3283.
Taylor, G. I. (1921), Diffusion by continuous movement, *Proc. London Math. Soc. Ser. A*, *20*, 196–221.
Tennekes, H., and J. L. Lumley (1972), *A First Course in Turbulence*, 1–300 pp., MIT Press, Cambridge, Mass.
Thompson, A. F. (2010), Jet formation and evolution in baroclinic turbulence with simple topography, *J. Phys. Oceanogr.*, *40*, 257–278.
Thompson, A. F., P. H. Haynes, C. Wilson, and K. J. Richards (2011), Rapid Southern Ocean front transitions in an eddy-resolving ocean GCM, *Geophys. Res. Lett.*, *37*, L23602, doi:10.1029/2010GL045386.
Toole, J. M. (1981), Intrusion characteristics in the Antarctic Polar Front, *J. Phys. Oceanogr.*, *6*, 780–793.
Traon, P. Y. L., Y. Faugère, F. Hernández, J. Dorandeu, F. Mertz, and M. Ablain (2003), Can we merge geosat follow-on with TOPEX/POSEIDON and ERS-2 for an improved description of the ocean circulation?, *J. Atmos. Oceanic Technol.*, *20*, 889–895.
Treguier, A. M. (1999), Evaluating eddy mixing coefficients from eddy-resolving ocean models: A case study, *J. Mar. Res.*, *57*, 89–108.
Visbeck, M., J. Marshall, T. Haine, and M. Spall (1997), On the specification of eddy transfer coefficients in coarse-resolution ocean circulation models, *J. Phys. Oceanogr.*, *27*, 381–402.
Waugh, D. W., and E. R. Abraham (2008), Stirring in the global surface ocean, *Geophys. Res. Lett.*, *35*, L20605, doi:10.1029/2008GL035526.
Weiss, J. (1991), The dynamics of enstrophy transfer in two-dimensional hydrodynamics, *Phys. D*, *48*, 273–294.
Wunsch, C. (1999), Where do ocean heat fluxes matter?, *J. Geophys. Res.*, *104*, 13,235–13,249.

R. Ferrari, Department of Earth, Atmospheric and Planetary Sciences, Massachusetts Institute of Technology, 77 Massachusetts Ave., Cambridge, MA 02139, USA.

A. C. Naveira Garabato, University of Southampton, National Oceanography Centre, European Way, Southampton SO14 3ZH, UK. (acng@noc.soton.ac.uk)

K. L. Polzin, Physical Oceanography Department, Woods Hole Oceanographic Institution, MS 21, Woods Hole, MA 02543, USA.